

**Searching for additional heating — [O II] emission in the diffuse ionized gas of  
NGC 891<sup>1</sup>, NGC 4631 and NGC 3079**

B. Otte<sup>2</sup>, R. J. Reynolds, J. S. Gallagher III<sup>2</sup>

*Department of Astronomy, University of Wisconsin–Madison*

*475 North Charter Street, Madison, WI 53706*

otte@astro.wisc.edu, reynolds@astro.wisc.edu, jsg@astro.wisc.edu

and

A. M. N. Ferguson

*Kapteyn Astronomical Institute, University of Groningen*

*P.O. Box 800, 9700 AV Groningen, The Netherlands*

ferguson@astro.rug.nl

**ABSTRACT**

We present spectroscopic data of ionized gas in the disk–halo regions of three edge–on galaxies, NGC 891, NGC 4631 and NGC 3079, covering a wavelength range from [O II]  $\lambda 3727\text{\AA}$  to [S II]  $\lambda 6716.4\text{\AA}$ . The inclusion of the [O II] emission provides new constraints on the properties of the diffuse ionized gas (DIG), in particular, the origin of the observed spatial variations in the line intensity ratios. We used three different methods to derive electron temperatures, abundances and ionization fractions along the slit. The increase in the [O II]/H $\alpha$  line ratio towards the halo in all three galaxies requires an increase either in electron temperature or in oxygen abundance. Keeping the oxygen abundance constant yields the most reasonable results for temperature, abundances, and ionization fractions. Since a constant oxygen abundance seems to require an increase in temperature towards the halo, we conclude that gradients in the electron temperature play a significant role in the observed variations in the optical line ratios from extraplanar DIG in these three spiral galaxies.

*Subject headings:* ISM: abundances — ISM: general — ISM: individual (NGC 891, NGC 3079, NGC 4631) — galaxies: abundances — galaxies: general — galaxies: individual (NGC 891, NGC 3079, NGC 4631)

## 1. INTRODUCTION

When examining ionized gas, it is common practice to distinguish between classical H II regions (Strömgren spheres around OB stars) and diffuse ionized gas (DIG), the gas outside the boundaries of the Strömgren spheres. While H II regions are created by photoionization, the ionization processes for the DIG are less well known. Many attempts have been made to explain the DIG by photoionization models (e.g. Domgörgen & Mathis 1994; Sokolowski 1992), while a few studies address the possibility of shock excitation (e.g. Sivan, Stasińska, & Lequeux 1986). In recent years, DIG was found not only in the disks of galaxies, but also far above the stellar disks in the halo of the Milky Way and in several edge-on galaxies at heights of more than 1 kpc (e.g. Reynolds 1985; Rand, Kulkarni, & Hester 1990). Questions therefore arise about where this extraplanar DIG (eDIG) comes from and how it is ionized.

Dynamical models of galaxies like ‘galactic fountains’ (Shapiro & Field 1976) and ‘chimneys’ (Norman & Ikeuchi 1989) describe how gas can be transported from the disk into the halo. Supernova explosions heating the gas in the disk and pushing it up into the halo are important for both the dynamics and the ionization of the gas in the halo. Due to the high velocities in this ejected gas, shocks can arise and ionize the gas far above the disk. The models of runaway O stars leaving the disk and moving into the halo (e.g. Gies 1987), leaking ionizing photons from the disk into the halo due to low density gas (Miller & Cox 1993; Dove & Shull 1994) as well as the theory of photons created by neutrino decay (Sciama 1990) are further attempts to explain the ionization of extraplanar DIG.

Both Martin (1997) and Rand (1998) were able to explain the run of several of the observed emission line ratios from H II regions to the DIG with composite models. Their models consisted of photoionization and one additional ionization process (shock ionization, turbulent mixing layers). This additional process was needed to explain the rise in the [O III]/H $\beta$  line ratio with increasing distance from the disk. However, even with these composite models it was not possible to explain the constant [S II]/[N II] line ratio, which was observed in NGC 891 (Rand 1998), as well as in the Milky Way (Haffner et al. 1999) and other galaxies (Otte & Dettmar 1999). These data led Haffner et al. (1999) to the conclusion that the electron temperature increases with increasing distance from the midplane of the galaxies.

A rise in temperature can explain both the growing [O III]/H $\beta$  ratio as well as the constant [S II]/[N II] ratio with increasing galactic altitude  $|z|$  without invoking an additional ionization mechanism at high  $|z|$ . Such a rise in electron temperature also should effect the [O II]/H $\alpha$  line ratio.

---

<sup>1</sup>Based on observations made with the William Herschel Telescope operated on the island of La Palma by the Isaac Newton Group in the Spanish Observatorio del Roque de los Muchachos of the Instituto de Astrofísica de Canarias.

<sup>2</sup>Visiting Astronomer, Kitt Peak National Observatory, National Optical Astronomy Observatories, which is operated by the Association of Universities for Research in Astronomy, Inc. (AURA) under cooperative agreement with the National Science Foundation.

The [O II]  $\lambda 3727\text{\AA}$  emission line provides important additional information about the ionization and heating processes in the DIG because of its high excitation energy. Below we present the results of observations of [O II], [O III], H $\beta$ , [N II], H $\alpha$ , and [S II] emission from the eDIG of three edge-on galaxies, NGC 891, NGC 4631 and NGC 3079. These objects represent the first targets of a small sample of edge-on galaxies which have been chosen for their known eDIG emission. The analysis of the other galaxies in our sample is still in progress. The results obtained from NGC 891, NGC 4631 and NGC 3079 provide some evidence for an increase in temperature with increasing height. Additional information is obtained about variations in the ionization state and chemical abundances within the gaseous halos.

## 2. OBSERVATIONS AND DATA REDUCTION

The spectra of NGC 891 were obtained with the ISIS spectrograph at the William Herschel 4.2 m Telescope on La Palma, Canary Islands, in 1999 September 10 under photometric conditions and dark skies. Gratings R316R and R300B were used for the red and the blue arm, respectively. Blocking filter GG495 was used for the red arm. The slitwidth was  $1''$ . The blue arm was read out in a 2x2 binned mode and yielded pixel scales of  $0''.40/\text{pixel}$  or  $1.74\text{\AA}/\text{pixel}$ . The covered wavelength range was from about  $3600\text{\AA}$  to  $5400\text{\AA}$ . The red arm was rebinned after reduction and calibration to match the spatial pixel scale of the blue arm. The wavelength dispersion for the red arm was  $1.47\text{\AA}/\text{pixel}$  with a wavelength range from about  $5700\text{\AA}$  to  $7200\text{\AA}$ . We combined two 30 min and one 20 min exposures in each arm. The slit position is the same as in Rand (1998) and shown in Figure 1.

The spectra of NGC 4631 and NGC 3079 were obtained with the GoldCam spectrograph at the 2.1 m telescope on Kitt Peak, AZ, in 2000 February 29 – March 6. We used grating 9 with decker 4 and a slitwidth of  $2''.5$ . This yielded a pixel scale of  $0''.80/\text{pixel}$  or  $2.44\text{\AA}/\text{pixel}$ , respectively, and a wavelength range from about  $3500\text{\AA}$  to  $7400\text{\AA}$ . We used filter WG345 to remove possible overlaps between orders. Exposure times varied from 20 min to 30 min depending on the weather. For NGC 4631, we combined eleven spectra with a total integration time of 4.5 hours. For NGC 3079, we combined nine spectra with a total integration time of 3 hours and 20 minutes. Both slit positions are perpendicular to the plane of the galaxies and shown in Figures 2 and 3. During the observations of galaxies, we also took a few spectra of blank sky regions.

The spectra were reduced using standard procedures in IRAF<sup>3</sup>. For sky subtraction, we subtracted differently scaled sky spectra from the red and the blue part of the galaxy spectra of NGC 4631 and NGC 3079. This was necessary for the spectra taken during the first night, which was partly cloudy. The sky spectra were smoothed along the slit by 15 pixels to increase the per-

---

<sup>3</sup>IRAF is distributed by the National Optical Astronomy Observatories, which are operated by the Association of Universities for Research in Astronomy, Inc., under cooperative agreement with the National Science Foundation.

pixel signal-to-noise ratios. The resulting spectra are of very good quality, and, in particular, we appear to have successfully removed the sky lines that can be confused with [O II] emission. For sky subtraction in our NGC 891 spectra, we averaged over about 100 rows in the galaxy spectra which did not show any galactic emission and used this average spectrum as sky. The spectra were then calibrated in wavelength and corrected for distortion using standard star exposures at different positions along the slit. After the flux calibration, we combined the spectra at each slit position by carefully examining the positions of emission lines in the wavelength direction and the position of flux features in the spatial direction. Individual spectra were shifted by integer pixels, if necessary, to overlap features and thus avoid broadening of lines and features during the combining procedure. The routine for cosmic ray removal during combining (averaging) of the spectra was insufficient. We therefore did not remove cosmic rays during image combining, but cleared the areas around emission lines of cosmic rays by hand later, before measuring emission lines. We only used galaxy spectra of comparable signal-to-noise for the combining procedure, that is we did not include spectra whose count rates were significantly reduced due to obscuration by clouds. Fortunately, for most spectra, the periods of cloud obscuration were short in comparison with the long exposure times. Thus, variations in the count rates of the galaxy emission were small and therefore negligible for most spectra. However, the variations in sky emission due to the clouds during our 2.1 m run could not be neglected, which we considered in our sky subtraction described above.

The analysis was done in MIDAS<sup>4</sup>. To measure emission lines, we fitted Gaussian curves to the emission lines at each row along the slit. We averaged each emission line along the slit, if necessary, to obtain a better signal-to-noise ratio in the halo. Usually, the measurements up to about 1.2 kpc above the disk were not averaged. For measurements between about 1.2 kpc and 2 kpc, we averaged over five rows in the spatial direction, which corresponds to 75 pc in NGC 891, 110 pc in NGC 4631, and 270 pc in NGC 3079. Above 2 kpc, we usually averaged over nine rows corresponding to 150 pc, 215 pc, and 540 pc, respectively. The averaging was done by comparing unaveraged measurements with averaged measurements to avoid smoothing out features in the emission line fluxes, i.e. our averaging should not have any effect on the derived line ratios.

The Balmer absorption lines could clearly be seen in the stellar continua around the Balmer emission lines  $H\beta$  and  $H\gamma$  (see Fig. 4). To correct for the underlying Balmer absorption lines, we assumed a constant equivalent width for these absorption lines and an intrinsic emission line intensity ratio of  $H\gamma/H\beta = 0.466$ . This procedure has been used, e.g., by Liu & Kennicutt (1995). We integrated the flux over a wavelength region which included the absorption line wings and could then determine the equivalent width with the assumptions mentioned above. The derived equivalent width was  $(4 \pm 1) \text{ \AA}$  along the slit. The color of the galaxy continua did not change significantly with height above the disk, suggesting that even at larger distances from the midplane, where no reliable  $H\gamma/H\beta$  ratios could be calculated, the equivalent width of the Balmer absorption lines did

---

<sup>4</sup>MIDAS is developed and maintained by the European Southern Observatory.

not change significantly either. All  $H\beta$  absorption lines seemed to be  $75 \pm 5 \text{ \AA}$  wide at the continuum level. We therefore fitted the  $H\beta$  absorption line using the derived equivalent width and the base width of  $75 \text{ \AA}$  to be able to correct our  $H\beta$  emission line fluxes for the underlying absorption. We did not try to correct the  $H\alpha$  emission for  $H\alpha$  absorption, because due to the low resolution, the  $H\alpha$  absorption line could not be observed, and was probably partially filled by  $[\text{N II}]$  emission. In all three galaxies, the  $H\alpha/H\beta$  line ratio decreases below the theoretical value of about 2.9 farther up in the halo at about 2 kpc. Since the  $H\beta$  emission becomes very faint at these heights, our absorption line correction seems to fail for very weak  $H\beta$  emission. We will therefore exclude data connected to  $H\alpha/H\beta < 2.9$  in our analysis.

The high values of  $H\alpha/H\beta$  in the midplane of the galaxies ( $H\alpha/H\beta \approx 8$  for NGC 891 and NGC 4631 and  $H\alpha/H\beta \approx 7$  for NGC 3079) also show that extinction correction in the disk was necessary. We derived the optical depth  $\tau$  from the  $H\alpha/H\beta$  line ratio and used the “usual” method for the extinction coefficients described in Mathis (1983). Figure 5 shows the line ratio  $[\text{O II}]/H\alpha$  for NGC 4631 without extinction correction (upper panel) and after extinction correction (lower panel). Due to the uncertainty of the extinction correction, it is not clear how physical the increase of the  $[\text{O II}]$  line ratio caused by the extinction correction really is. We did not estimate any error for the extinction correction, i.e. the error bars of the line ratios only reflect the errors of our flux measurements. The maximum extinction correction yielded a factor of 9–12 for  $[\text{O II}]$  (!), a factor of 2.6–3.0 for  $H\beta$ , and a factor of 2.4–2.7 for  $[\text{O III}]$ , whereas the red lines had factors of about 1. Since we were interested in the change of the line ratios and the physical properties with increasing distance from the midplane, it was important to keep in mind which values were affected the most and in what way by the extinction correction.

### 3. RESULTS

For all three galaxies (NGC 891, NGC 4631, NGC 3079), we wanted to fit the line ratios  $[\text{O II}]/H\alpha$ ,  $[\text{O III}]/H\alpha$ ,  $[\text{N II}]/H\alpha$  and  $[\text{S II}]/H\alpha$  from the eDIG. Since each line ratio depends on element abundance, ionization fraction and temperature, we had to make a few assumptions to decrease the number of unknowns: 1) We assumed that all the emitting gas is ionized. This means in particular that  $\text{H}^+/\text{H} = 1$ . 2) Since the ionization potentials of neutral nitrogen and oxygen are similar, we assumed that the ionization fractions of both elements are the same for singly ionized atoms, i.e.  $\text{N}^+/\text{N} = \text{O}^+/\text{O}$  (e.g. Sembach et al. 2000). 3) It has been observed in several objects that the ratio of the oxygen abundance to the sulfur abundance is about 100/3, independent of metallicity (Mathis 2000). We adopted this ratio to derive the sulfur abundance from the oxygen abundance. 4) We assumed that  $\text{O}^{+++}/\text{O}$  (and higher ionization stages of oxygen) is negligibly small and therefore  $(\text{O}^+/\text{O}) + (\text{O}^{++}/\text{O}) = 1$ . (No assumptions were made for doubly ionized sulfur or doubly ionized nitrogen, i.e. we did not derive nor use these ionization fractions.) 5) One additional assumption was necessary, which yielded three different fitting methods. We adopted a constant ionization fraction  $\text{O}^{++}/\text{O}$  along the slit (Method A), a constant temperature along the

slit (Method B), and a constant oxygen abundance along the slit (Method C). In the following, we will discuss each method and its results in more detail.

### 3.1. Method A: $O^{++}/O=\text{const.}$

For each fitting method, we started with the  $[O\ II]/[O\ III]$  line ratio, because it depends only on temperature and ionization fractions, but not on abundance. Due to the low resolution in our spectra, we were not able to distinguish between  $[O\ II]\ \lambda 3726.0\text{\AA}$  and  $[O\ II]\ \lambda 3728.8\text{\AA}$ . Thus, we use  $[O\ II]\ \lambda 3727\text{\AA}$  to mean the sum of both  $[O\ II]$  doublet lines. The  $[O\ II]/[O\ III]$  line ratio can be written as

$$\frac{I_{3727}}{I_{5006.9}} = 2.49 e^{-0.99/T_4} \left(\frac{O^+}{O}\right) \left(\frac{O^{++}}{O}\right)^{-1} \quad (1)$$

(Osterbrock 1989). All line ratio equations contain intensities in  $\text{ergs s}^{-1} \text{cm}^{-2} \text{sr}^{-1}$  with  $T_4$  being the electron temperature in 10 000 K.

We tried four different ionization fractions for  $O^{++}/O$  (0.05, 0.10, 0.15 and 0.20) to cover a reasonable range and calculated the electron temperature for each case from equation (1). We then used the  $[O\ III]/H\beta$  line ratio

$$\frac{I_{5006.9}}{I_{4861.3}} = 5.03 \cdot 10^5 T_4^{0.33} e^{-2.88/T_4} \left(\frac{O^{++}}{O}\right) \left(\frac{O}{H}\right) \left(\frac{H^+}{H}\right)^{-1} \quad (2)$$

(Osterbrock 1989) to derive the oxygen abundance  $O/H$  for each case. With the assumption of similar ionization fractions for nitrogen and oxygen as mentioned earlier, we could derive the nitrogen abundances from the  $[O\ II]/[N\ II]$  line ratio

$$\frac{I_{3727}}{I_{6583.4}} = 2.65 e^{-1.69/T_4} \left(\frac{O^+}{O}\right) \left(\frac{O}{H}\right) \left(\frac{N^+}{N}\right)^{-1} \left(\frac{N}{H}\right)^{-1} \quad (3)$$

(Osterbrock 1989). We also could derive the ionization fractions of singly ionized sulfur for each case by assuming the ratio  $O/S$  to be 100/3 (as mentioned above) and using the  $[O\ II]/[S\ II]$  line ratio

$$\frac{I_{3727}}{I_{6716.4}} = 0.58 e^{-1.73/T_4} \left(\frac{O^+}{O}\right) \left(\frac{O}{H}\right) \left(\frac{S^+}{S}\right)^{-1} \left(\frac{S}{H}\right)^{-1} \quad (4)$$

(Osterbrock 1989). The final step now was to compare the observed  $H\alpha$  line ratios with the predicted ratios based upon the derivations above:

$$[O\ II]/H\alpha : \frac{I_{3727}}{I_{6562.8}} = 4.31 \cdot 10^5 T_4^{0.4} e^{-3.87/T_4} \left(\frac{O^+}{O}\right) \left(\frac{O}{H}\right) \left(\frac{H^+}{H}\right)^{-1} \quad (5)$$

$$[O\ III]/H\alpha : \frac{I_{5006.9}}{I_{6562.8}} = 1.74 \cdot 10^5 T_4^{0.4} e^{-2.88/T_4} \left(\frac{O^{++}}{O}\right) \left(\frac{O}{H}\right) \left(\frac{H^+}{H}\right)^{-1} \quad (6)$$

$$[N\ II]/H\alpha : \frac{I_{6583.4}}{I_{6562.8}} = 1.62 \cdot 10^5 T_4^{0.4} e^{-2.18/T_4} \left(\frac{N^+}{N}\right) \left(\frac{N}{H}\right) \left(\frac{H^+}{H}\right)^{-1} \quad (7)$$

$$[\text{S II}]/\text{H}\alpha : \frac{I_{6716.4}}{I_{6562.8}} = 7.49 \cdot 10^5 T_4^{0.4} e^{-2.14/T_4} \left(\frac{S^+}{S}\right) \left(\frac{S}{H}\right) \left(\frac{H^+}{H}\right)^{-1} \quad (8)$$

(Osterbrock 1989; Haffner, Reynolds, & Tufte 1999).

The derived values for electron temperature, oxygen and nitrogen abundances and for the ionization fraction of sulfur, as well as the fitted line ratios, are shown for NGC 891 in Figure 6, for NGC 4631 in Figure 7 and for NGC 3079 in Figure 8. Since the [O III] and H $\beta$  emission lines were fainter than the other emission lines in the spectra, the line ratio fits, which are based on these lines, usually do not extend as far out into the halo as the observed line ratios. The predicted H $\alpha$  line ratios using different ionization fractions for doubly ionized oxygen do not differ from each other very much. However, the derived temperatures, abundances and sulfur ionization fractions are quite sensitive to the ionization fraction of oxygen. This is true for all three galaxies.

The line ratio predictions for NGC 891 match the observed line ratios quite well. The peaks in the [O II]/H $\alpha$  line ratio in the midplane were enhanced by the uncertain internal extinction corrections. In NGC 891, the range in height from the midplane affected by internal extinction is about  $|z| \leq 1200$  pc. Our [N II]/H $\alpha$  line ratios match those observed by Collins & Rand (2001) at the same slit position. However, our [S II]/H $\alpha$  line ratios are higher below the disk (1.0 at  $z = -2$  kpc as opposed to 0.6), but the same above the disk (0.6 at  $z = +2$  kpc). Our [O III]/H $\alpha$  measurements are slightly higher at  $|z| = 2$  kpc than the values measured by Collins & Rand, but certainly comparable within the error bars. However, Collins & Rand did not measure as high a peak in [O III]/H $\alpha$  at  $z \approx 200$  pc as we did.

In NGC 4631, the line ratio predictions also match the observed line ratios. The peaks in [O II]/H $\alpha$  at  $z \approx -1200$  pc,  $z \approx -600$  pc and  $z \approx -300$  pc were all introduced by the extinction correction. The line ratio predictions for NGC 3079 seem to match the observed line ratios as well. However, in the range  $-2200$  pc  $< z < -600$  pc, the H $\beta$  emission line in the underlying Balmer absorption line could not clearly be distinguished from the noise. Therefore, it was not possible to predict line ratios in this part of the slit. And the derived optical depth for the extinction correction and with it the [O II]/H $\alpha$  and [O III]/H $\alpha$  line ratios are rather questionable in this range. Unfortunately, the nitrogen line at 6583.4 Å had been hit by cosmic rays in the range  $-3.4$  kpc  $< z < -2.6$  kpc and  $+1.4$  kpc  $< z < +2.2$  kpc, which then contaminated the [N II]/H $\alpha$  line ratio in these areas. Also, the [O III] emission line at 5006.9 Å had been hit by a cosmic ray at  $z < -2.8$  kpc.

In all three galaxies, the derived abundances for oxygen and nitrogen are higher than solar by up to four orders of magnitude for the ionization fraction  $\text{O}^{++}/\text{O} = 0.05$ . These abundances seem unlikely, because it is difficult to obtain higher abundances farther away from star forming regions, especially in the halo. The ionization fraction  $\text{O}^{++}/\text{O} = 0.15$  and  $0.20$  yielded sulfur ionization fractions close to or greater than unity. This is unlikely (or even impossible) given the low (23 eV) ionization potential of S $^+$  and the significant amount of S $^{++}$  predicted by photoionization models (e.g. Mathis 1986). The electron temperature seems to be constant in the halo in all three galaxies

with higher values in the area affected by the extinction correction. The only oxygen ionization fraction with reasonable values for all derived properties is  $O^{++}/O = 0.10$ , except for  $S^+/S$  in NGC 891. No reasonable solution seems to exist for NGC 891 using Method A.

### 3.2. Method B: $T_4=\text{const.}$

For the next method, we assumed a constant electron temperature along the slit and derived the ionization fraction of oxygen from equation (1). We tried four different temperatures ( $T_4 = 0.4, 0.6, 0.8$  and  $1.0$ ). For each temperature, we derived the oxygen and nitrogen abundances and the sulfur ionization fraction using equations (2)–(4). We then compared the observed line ratios relative to  $H\alpha$  with the ratios predicted by equations (5)–(8). The predictions fit the observations as well as in Method A and therefore are not shown here. However, the derived values for ionization fractions and abundances again vary considerably from case to case as shown in Figures 9–11.

The lowest electron temperature ( $T_4 = 0.4$ ) yielded nitrogen and oxygen abundances one or two orders of magnitude above solar in all three galaxies. Even  $T_4 = 0.6$  produced oxygen abundances above solar, whereas the nitrogen abundances have approximately solar values. The highest temperature ( $T_4 = 1.0$ ) caused very high or unreasonable sulfur ionization fractions in the halo of the galaxies.  $S^+/S$  is still somewhat high for  $T_4 = 0.8$  in NGC 891. Therefore, we find the most reasonable values for abundances and ionization fractions for an electron temperature of  $T_4 \approx 0.7$ . By keeping the electron temperature constant, the nitrogen abundances increase towards the halos in all three galaxies, whereas the oxygen abundance increases slightly or almost stays constant with increasing distance from the midplane.

### 3.3. Method C: $O/H=\text{const.}$

Our last fitting method differs a little from the previous two methods. We combined equations (1) and (2) to eliminate the dependence on the ionization fractions of oxygen.  $[O\ III]/H\beta$  becomes

$$\frac{[O\ III]}{H\beta} = \frac{5.03 \cdot 10^5 \cdot T_4^{0.33} \cdot e^{-2.88/T_4}}{[O\ II]/[O\ III] \cdot 0.40 \cdot e^{0.99/T_4} + 1} \cdot \left(\frac{O}{H}\right). \quad (9)$$

We assumed solar abundance for oxygen ( $O/H = 8.5 \cdot 10^{-4}$  (Däppen 2000)). We then calculated the minimum and maximum allowed electron temperature for each data point along the slit by fitting the observed  $[O\ III]/H\beta$  line ratios within their  $1\sigma$  error bars using temperature increments/decrements of 400 K. For both temperature extremes, we derived the nitrogen abundances and the oxygen and sulfur ionization fractions using equations (2)–(4) and compared the predicted with the observed  $H\alpha$  line ratios as usual.

The results for the three galaxies are shown in Figures 12–14. We included calculations for each galaxy which were not corrected for extinction to show how sensitive the predicted line ratios as

well as the derived properties are to extinction corrections. For all three galaxies, the predicted line ratios using the minimum electron temperature are generally too low in the halo in comparison with the observed values. However, the maximum allowed temperature fits are within the  $1\sigma$  error bars of the observed  $H\alpha$  line ratios ( $[O\ III]/H\alpha$ ,  $[N\ II]/H\alpha$ ) or slightly above ( $[O\ II]/H\alpha$ ,  $[S\ II]/H\alpha$ ) in the halo. Subtracting about a fourth of the difference between maximum and minimum temperature from the maximum allowed temperature seems to fit the line ratios best. The only exception is for the uncorrected line ratios below the disk of NGC 4631 (down to  $z = -1400$  kpc), where the predicted line ratios of both minimum and maximum electron temperature are too high for all four line ratios. We point out that the previously derived optical depth is greater than zero in this region. In general, the extinction corrected line ratios and their predictions match better than the not extinction corrected values in areas where the derived  $\tau > 0$ . This is especially true for the region around the midplane of each galaxy.

The derived nitrogen abundances are close to solar for both temperatures in all three galaxies. The sulfur ionization fractions are below unity for both temperature ranges in NGC 891, NGC 4631 and NGC 3079, but exceed unity in the uncorrected case of NGC 891. The comparison between the extinction corrected values and the uncorrected values for each galaxy shows clearly, how strongly the extinction correction affects the derived properties, in particular the nitrogen abundances and the sulfur ionization fractions.

In all three galaxies, the extinction corrected values of  $S^+/S$  increase with  $|z|$ , where  $\tau > 0$ , and then decrease or stay constant, where  $\tau = 0$ . The uncorrected values of  $S^+/S$  decrease with  $|z|$  (NGC 891, NGC 3079) or stay constant (NGC 4631). The same behaviour can be seen in the nitrogen abundance of each galaxy, i.e. increase with  $|z|$ , where  $\tau > 0$ , and then decrease in  $N/H$  or constant  $N/H$ , where  $\tau = 0$ , and decrease with  $|z|$  or constant  $N/H$  in the uncorrected cases. In the extinction corrected calculations,  $O^{++}/O$  more or less increases with distance from the midplane in all three galaxies. In the uncorrected cases,  $O^{++}/O$  slightly increases with  $|z|$  in NGC 891 and basically stays constant in NGC 4631 and NGC 3079.

The electron temperature stays constant or increases with  $|z|$  in all three galaxies (not considering the peaks introduced by the extinction correction). In NGC 891,  $T_4$  stays overall constant within the range affected by the extinction correction ( $|z| \leq 1200$  pc) and then starts to increase with  $z$  at least above the disk ( $z > +1200$  pc). Below the disk, no obvious increase is observed. In the uncorrected case of NGC 891, the electron temperature starts to increase already at  $|z| = 400$  pc from  $T_4 \approx 0.6$  to  $T_4 \approx 0.72$  at  $z = +1600$  pc and from  $T_4 \approx 0.56$  to  $T_4 \approx 0.69$  at  $z = -1.8$  kpc (considering the average of minimum and maximum allowed electron temperature).

In NGC 4631, the extinction correction affects the range of  $-1400$  pc  $< z < 1000$  pc. Beyond this range in height, the electron temperature increases from  $T_4 \approx 0.7$  to  $T_4 \approx 0.8$  above the disk. Below the disk, the electron temperature may slightly increase from  $T_4 \approx 0.73$  to  $T_4 \approx 0.8$  at  $z = -2$  kpc. However, the temperature may also be constant in this area given the range set by minimum and maximum allowed temperature. In the uncorrected case of NGC 4631, the

temperature increase is more obvious at least above the disk, ranging from  $T_4 \approx 0.66$  at  $z = +500$  pc to  $T_4 \approx 0.8$  at  $z = +2$  kpc. Below the disk, the temperature seems to increase from  $T_4 \approx 0.72$  at  $z = -1$  kpc to  $T_4 \approx 0.8$  at  $z = -2$  kpc. However, the temperature may be constant in this area considering the difference between minimum and maximum allowed temperature.

The electron temperature seems to stay more or less constant below the disk of NGC 3079 (ignoring the increase between  $z = 0$  and  $z = -1$  kpc enhanced by the extinction correction). The temperature slightly increases with  $z$  above the disk (from  $T_4 = 0.67$  at  $z = 0$  to  $T_4 = 0.78$ ). In the uncorrected case of NGC 3079, the electron temperature increases from  $T_4 = 0.6$  at  $z = 0$  to  $T_4 \approx 0.78$  at  $z = +2$  kpc and  $T_4 \approx 0.7$  at  $z = -2.8$  kpc. However, the variations (wiggles) in the temperatures in NGC 3079 are larger relative to the increase in  $T_4$  than in the two other galaxies, making the temperature increases less convincing in NGC 3079 than in NGC 891 and NGC 4631. We point out that there is no temperature decrease with increasing distance from the midplane in any of the discussed cases.

The disadvantage of using the [O II], [O III] and  $H\beta$  emission lines for the derivation of  $T_4$  is obviously the dependence on the extinction correction. However, this dependence becomes less and even negligibly small in the halo with increasing distance from the midplane. The advantage of using the blue emission lines to derive the electron temperature is the stronger dependence of the [O II]/[O III] and [O III]/ $H\beta$  line ratios on  $T_4$ , i.e. these line ratios are more sensitive to the electron temperature than the [N II]/ $H\alpha$  line ratio used by Haffner et al. (1999) or Collins & Rand (2001). Our (averaged) temperatures for NGC 891 are 1300 K–1600 K lower in the halo and 500 K–900 K lower in the disk than those derived by Collins & Rand (again ignoring the peaks introduced by our extinction correction).

Since the assumption of solar oxygen abundance yielded already reasonable values for temperature, nitrogen abundance and ionization fractions, we did not use this method with other values for the oxygen abundance.

#### 4. DISCUSSION

The overall trends of the  $H\alpha$  line ratios in NGC 891, NGC 4631 and NGC 3079 are the same as those in other galaxies, i.e. [S II]/ $H\alpha$ , [N II]/ $H\alpha$  and [O III]/ $H\alpha$  increase with increasing height. [O II]/ $H\alpha$  also increases with distance from the midplane. In NGC 3079, the overall emission is fainter than in NGC 4631 and NGC 891.

The [S II]/[N II] line ratio in NGC 891 (Fig. 15, top panel) stays constant from about  $z = -1400$  pc to about  $z = +2600$  pc at a value of  $0.55 \pm 0.10$ . It matches the value measured by Collins & Rand (2001). The [O II]/[N II] line ratio increases towards the halo in the extinction corrected case (at  $|z| > 1$  kpc, Fig. 15, middle panel) as well as the uncorrected case (at  $|z| > 200 - 400$  pc, Fig. 15, bottom panel). These results are consistent with the variations in electron temperature in the extraplanar diffuse ionized gas found by the analysis in section 3 above. These temperature

variations leave the  $[\text{S II}]/[\text{N II}]$  ratio in the eDIG basically unchanged, because this ratio is almost independent of electron temperature, whereas the strongly electron temperature dependent ratio  $[\text{O II}]/[\text{N II}]$  increases with  $|z|$ . Changes in the ionization fractions may cause the smaller scale variations of  $[\text{S II}]/[\text{N II}]$  and  $[\text{O II}]/[\text{N II}]$  along the slit.

In NGC 4631, one unusual area is the H II region at about 1 kpc below the disk. Its  $[\text{S II}]/\text{H}\alpha$  and  $[\text{N II}]/\text{H}\alpha$  line ratios are lower than those of the surrounding diffuse gas (as expected by photoionization), whereas the  $[\text{O III}]/\text{H}\alpha$  ratio only increases in one part of the H II region (at  $z \approx -800$  pc), but not in the other part (at  $z \approx -1$  kpc). More observations are necessary to understand this particular region. The line ratio  $[\text{S II}]/[\text{N II}]$  (Fig. 16, top panel) seems to stay constant with increasing height in NGC 4631 ( $0.8 \pm 0.1$  above  $z = +1$  kpc and  $1.0 \pm 0.2$  below  $z = +300$  pc). In the midplane, the value decreases to a minimum of 0.55 at about  $z = +500$  pc. However, the strong variations in electron temperature (up to 5000 K) below the disk as derived in section 3 are big enough to enhance the variations below the disk even in the almost temperature independent line ratio  $[\text{S II}]/[\text{N II}]$ .

The middle panel in Fig. 16 shows the extinction corrected  $[\text{O II}]/[\text{N II}]$  line ratio in NGC 4631, the bottom panel shows the uncorrected line ratio. In the extinction corrected case, the variations in the  $[\text{O II}]/[\text{N II}]$  line ratio below the disk are caused by variations in electron temperature according to our analysis above (Method C). In the uncorrected case, the  $[\text{O II}]/[\text{N II}]$  line ratio seems to stay constant below the disk except for the unusual H II region mentioned above. The variations in electron temperature seem to be compensated by strong variations in nitrogen abundance below the disk. Above the disk, the  $[\text{O II}]/[\text{N II}]$  line ratio first stays constant ( $+1000$  pc  $< z < +1600$  pc) and then increases with  $z$  up to  $z = +2$  kpc (in both the extinction corrected and the uncorrected case). According to our results from Method C, this behaviour can be explained by a steady increase in electron temperature combined with an increase in nitrogen abundance up to  $z = +1600$  pc and a decrease in N/H between 1600 pc and 2000 pc. Unfortunately, since our derived values for  $\text{H}\alpha/\text{H}\beta$  drop below 2.9 at  $z = +2$  kpc, we do not have reliable estimates for abundances or ionization fractions in this area and therefore cannot explain the decrease in  $[\text{O II}]/[\text{N II}]$  at  $z > +2$  kpc. Due to a superbubble above the disk of NGC 4631 (Hoopes, Walterbros, & Rand 1999), the conditions in the eDIG might be different from those below the disk, resulting in the lower, but still constant  $[\text{S II}]/[\text{N II}]$  ratio (in comparison with the area below the disk) and the slower increase of  $[\text{O II}]/[\text{N II}]$  towards the halo (in comparison with the observed increase in NGC 891), assuming that the temperature still dominates over photoionization in the superbubble region.

The  $[\text{S II}]/[\text{N II}]$  ratio in NGC 3079 (Fig. 17, top panel) stays constant with increasing height above the disk ( $5.3 \pm 0.7$  at  $z > +200$  pc), except for the area affected by the cosmic ray. However, below the disk, the ratio first increases with height (from 0.45 at  $z = 0$  to about 1.2 at  $z = -1.5$  kpc), then decreases over a short distance to about 0.6 at  $z = -1.8$  kpc. Beyond that point,  $[\text{S II}]/[\text{N II}]$  seems to increase again with distance from the midplane. Unfortunately, we could not determine abundances or ionization fractions between  $-2$  kpc and  $-800$  pc because of too faint  $\text{H}\beta$  emission.

The middle panel in Fig. 17 shows the extinction corrected  $[\text{O II}]/[\text{N II}]$  line ratio in NGC 3079 along the slit, the bottom panel again shows the uncorrected line ratio. In both cases, the line ratio increases with distance from the midplane below the disk ( $z < -1800$  pc). Above the disk,  $[\text{O II}]/[\text{N II}]$  seems to stay constant or to slightly decrease with  $z$  at  $z > +600$  pc. According to our Method C, the decrease in  $[\text{O II}]/[\text{N II}]$  between  $z = 0$  and  $z = +1400$  pc in the extinction corrected case is caused by an increase in nitrogen abundance (about a factor of 2), while the electron temperature increases only slightly. In the uncorrected case,  $[\text{O II}]/[\text{N II}]$  first increases between  $z = 0$  and  $z = +600$  pc, caused by an increase in electron temperature combined with a decrease in nitrogen abundance, and then stays more or less constant up to  $z = +1400$  pc. Neither electron temperature nor nitrogen abundance vary significantly between  $z = +600$  pc and  $z = +1400$  pc.

In all three galaxies, the behaviour of  $[\text{S II}]/[\text{N II}]$  and  $[\text{O II}]/[\text{N II}]$  can also be explained by variations of several orders of magnitude in the abundances (according to our results of Method A) or variations in the abundances combined with strong variations in the ionization fractions (according to our results of Method B).

The question now is which of the three fitting methods yields the most reasonable results. The best predictions in Method A ( $\text{O}^{++}/\text{O} = \text{const.}$ ) are produced, if the ionization fraction  $\text{O}^{++}/\text{O} = 0.10$ . This is true for two of our three galaxies. However, even with this value, the derived abundances are rather unlikely, because they vary by more than one order of magnitude along the slit. Moreover, it is difficult, if not impossible to obtain oxygen and nitrogen abundances below or equal to solar along the entire slit without exceeding unity for  $\text{S}^+/\text{S}$ .

In Method B ( $T_4 = \text{const.}$ ), the most reasonable value for  $T$  appears to be 7000 K. However, the requirement of a non-varying temperature causes an increase in abundance away from the midplane, although the resulting spread in oxygen and nitrogen abundances are less than for Method A. The values for  $\text{N}/\text{H}$  are below or close to solar in all three galaxies along the slit for electron temperatures of about 7000 K. The oxygen abundance is about solar along the slit (slightly higher for NGC 4631), but probably reaches higher than solar values in the halo according to the slight increase of  $\text{O}/\text{H}$  with  $|z|$ . The abundances increase with increasing distance from the disk. To achieve this abundance gradient, outflows or chimneys with stable chimney walls are needed. In this scenario, the metal rich gas from the disk is blown into the halo to heights where the density of the ambient medium is low enough that mixing can occur, while the higher density and higher pressure along the sides of the outflows prevent the mixing of gas. However, it is rather unlikely that only powerful outflows occur which can reach far up into the halo and enrich the halo gas, while the diffuse gas near the disk retains lower metal abundances. It is more likely that there are many more smaller scale outflows than large scale ones, so that the halo gas near the disk becomes more metal enriched than the halo gas farther away from the disk.

The nitrogen abundances in Method C ( $\text{O}/\text{H} = \text{const.}$ ) are about solar or below along the slit in NGC 4631 and NGC 3079. In NGC 891,  $\text{N}/\text{H}$  reaches twice the solar value in the extinction corrected case and higher values in the uncorrected case. The variations in  $\text{N}/\text{H}$  are smaller than

the corresponding values of Method A and B. N/H stays constant or decreases with increasing distance from the midplane (ignoring the overcorrected values of the extinction correction). The gradient is consistent with the hypothesis of stars in the disk enriching the gas around them and the gravitational potential of the disk keeping the enriched gas near the disk. An almost constant abundance would be a sign of well-mixed gas.

The behaviour of the sulfur ionization fraction  $S^+/S$  depends strongly on the extinction correction.  $S^+/S$  seems to stay constant (NGC 4631, NGC 3079) or to decrease (NGC 891) with increasing distance from the midplane, where  $\tau = 0$ . A decrease in  $S^+/S$  with  $|z|$  would indicate an increase in  $S^{++}/S$  and thus an additional source of ionization for the halo gas. The ionization potential for  $O^{++}$  is higher than that for  $S^{++}$  (35 eV and 23 eV, respectively). Therefore, the ionization fraction of doubly ionized sulfur should be at least as high as that of doubly ionized oxygen, and thus  $(S^+/S) + (O^{++}/O) \leq 1$  along the slit. This seems to be the case in all three galaxies for  $T_4 = 0.7$  in Method B and temperatures close to, but below the maximum allowed temperatures along the slits in Method C. For the most reasonable ionization fraction  $O^{++}/O = 0.10$  in Method A, this condition is violated at a few data points in NGC 4631 and NGC 3079 and almost everywhere along the slit in NGC 891. The maximum temperatures reached in the halos of the galaxies in Method C are consistent with temperatures observed in other galaxies and the Milky Way ( $T_4 \approx 0.7 - 0.9$ ).

Photoionization models that use a decreasing ionization parameter with increasing  $|z|$  predict a decrease in  $O^{++}/O$  and an increase in  $S^+/S$  with increasing distance from the midplane (Sembach et al. 2000). We do not observe a decrease in electron temperature in any of our methods. An increasing electron temperature towards the halo appears to require an additional heating mechanism. If a harder source of ionization caused the observed constant or increasing temperatures towards the halo,  $O^{++}/O$  would have to be constant or to increase as well. We are not able to draw reliable conclusions about the behaviour of the ionization fractions, as they can be completely alternated by the applied extinction correction. However, the mostly constant  $[S \text{ II}]/[N \text{ II}]$  line ratios we observed rule out any additional heating mechanisms that also ionize the gas. Possible mechanisms which heat, but do not ionize the gas are dissipation of turbulence, grain heating, Coulomb collisions of cosmic rays, and magnetic field reconnections (Reynolds, Haffner, & Tufte 2000).

The eDIG in the three galaxies we observed behaves similarly within each method, even though the derived values for abundances, ionization fractions and temperatures differ slightly, and each galaxy also shows some peculiarities. Given these observations and derivations, Method C yields the most reasonable values, that is, a relatively uniform, near solar abundance distribution within the galaxies (except NGC 891). The extinction correction is questionable, with indications that it overcorrects near the midplane in the blue part of the spectrum; however, some correction is necessary given the high  $H\alpha/H\beta$  line ratios in the disk. The extinction also raises the question whether the emission of all the spectral lines originated in the same spatial region in the galaxies or whether for example the  $[O \text{ II}]$  photons we observed were emitted from different gas clouds than the  $H\beta$  photons. Thus, the true values for the emission line ratios and the derived properties near

the midplane may differ from those shown here, but we expect the errors will not be large ones at least in the halo. The key questions therefore are how high the midplane peaks in the  $[\text{O II}]/\text{H}\alpha$  line ratios really become and what causes them. Faint  $[\text{O I}]$  emission also appears to be present in the eDIG of NGC 4631 and NGC 3079, suggesting that neutral gas is present beyond the disks of these galaxies. Unfortunately, this emission is too faint to measure from our data.

## 5. CONCLUSIONS

We explored three different methods to explain the observed line ratio variations in the three galaxies, NGC 891, NGC 4631 and NGC 3079. Overall, one can say that the line ratios require either a constant or increasing electron temperature within the eDIG towards the halos, or an increase in abundances. Assuming a constant (near solar) oxygen abundance along the slit (our Method C, section 3.3) yields the most reasonable values for ionization fractions, abundances and temperature of these three methods. The derived values contradict pure photoionization models. We conclude therefore that variations in the electron temperature play a significant role in observed variations in the optical line intensity ratios from the eDIG in these three galaxies.

B. O. is thankful to the staff on Kitt Peak for their support during the observations. She is also grateful to S. Jansen for his computer support. The authors thank R. J. Rand for information on his NGC 891 data and the referee R. A. M. Walterbos for his comments and suggestions resulting in an improved paper. This research was funded by the NSF through grant AST96–19424 and in part by the Graduate School of the University of Wisconsin–Madison. The observing run at the 2.1 m was funded in part by the National Optical Astronomy Observatory. The Digitized Sky Surveys were produced at the Space Telescope Science Institute under U. S. Government grant NAGW-2166. The images of these surveys are based on photographic data obtained using the Oschin Schmidt Telescope on Palomar Mountain. The National Geographic Society – Palomar Observatory Sky Atlas was made by the California Institute of Technology with grants from the National Geographic Society. The Second Palomar Observatory Sky Survey was made by the California Institute of Technology with funds from the National Science Foundation, the National Geographic Society, the Sloan Foundation, the Samuel Oschin Foundation, and the Eastman Kodak Corporation. The Oschin Schmidt Telescope is operated by the California Institute of Technology and Palomar Observatory. Supplemental funding for sky–survey work at the STScI is provided by the European Southern Observatory.

## REFERENCES

- Collins, J. A., Rand, R. J. 2001, *ApJ* 551, 57
- Däppen, W. 2000, in *Allen’s Astrophysical Quantities*, ed. A. N. Cox (New York: Springer), 27

- Domgörgen, H., Mathis, J. S. 1994, ApJ 428, 647
- Dove, J. B., Shull, J. M. 1994, ApJ 430, 222
- Gies, D. R. 1987, ApJS 64, 545
- Haffner, L. M. 1998, PhD-thesis, University of Wisconsin–Madison, USA
- Haffner, L. M., Reynolds, R. J., Tufte, S. L. 1999, ApJ 523, 223
- Hoopes, C. G., Walterbos, R. A. M., Rand, R. J. 1999, ApJ 522, 669
- Liu, C. T., Kennicutt, R. C., Jr. 1995, ApJ 450, 547
- Martin, C. L. 1997, ApJ 491, 561
- Mathis, J. S. 1983, ApJ 267, 119
- Mathis, J. S. 1986, ApJ 301, 423
- Mathis, J. S. 2000, in Allen’s Astrophysical Quantities, ed. A. N. Cox (New York: Springer), 523
- Miller, W. W., Cox, D. P. 1993, ApJ 417, 579
- Norman, C. A., Ikeuchi, S. 1989, ApJ 345, 372
- Osterbrock, D. E. 1989, Astrophysics of Gaseous Nebulae and Active Galactic Nuclei (Mill Valley: University Science Books)
- Otte, B., Dettmar, R.–J. 1999, A&A 343, 705
- Rand, R. J. 1998, ApJ 501, 137
- Rand, R. J., Kulkarni, S. R., Hester, J. J. 1990, ApJ 352, L1
- Reynolds, R. J. 1985, ApJ 294, 256
- Reynolds, R. J., Haffner, L. M., Tufte, S. L. 2000, RMxAC 9, 249
- Sciama, D. W. 1990, ApJ 364, 549
- Sembach, K. R., Howk, J. C., Ryans, R. S. I., Keenan, F. P. 2000, ApJ 528, 310
- Shapiro, P. R., , Field, G. B. 1976, ApJ 205, 762
- Sivan, J.–P., Stasińska, G., Lequeux, J. 1986, A&A 158, 279
- Sokolowski, J. 1992, PhD Thesis, Rice University, Houston, TX

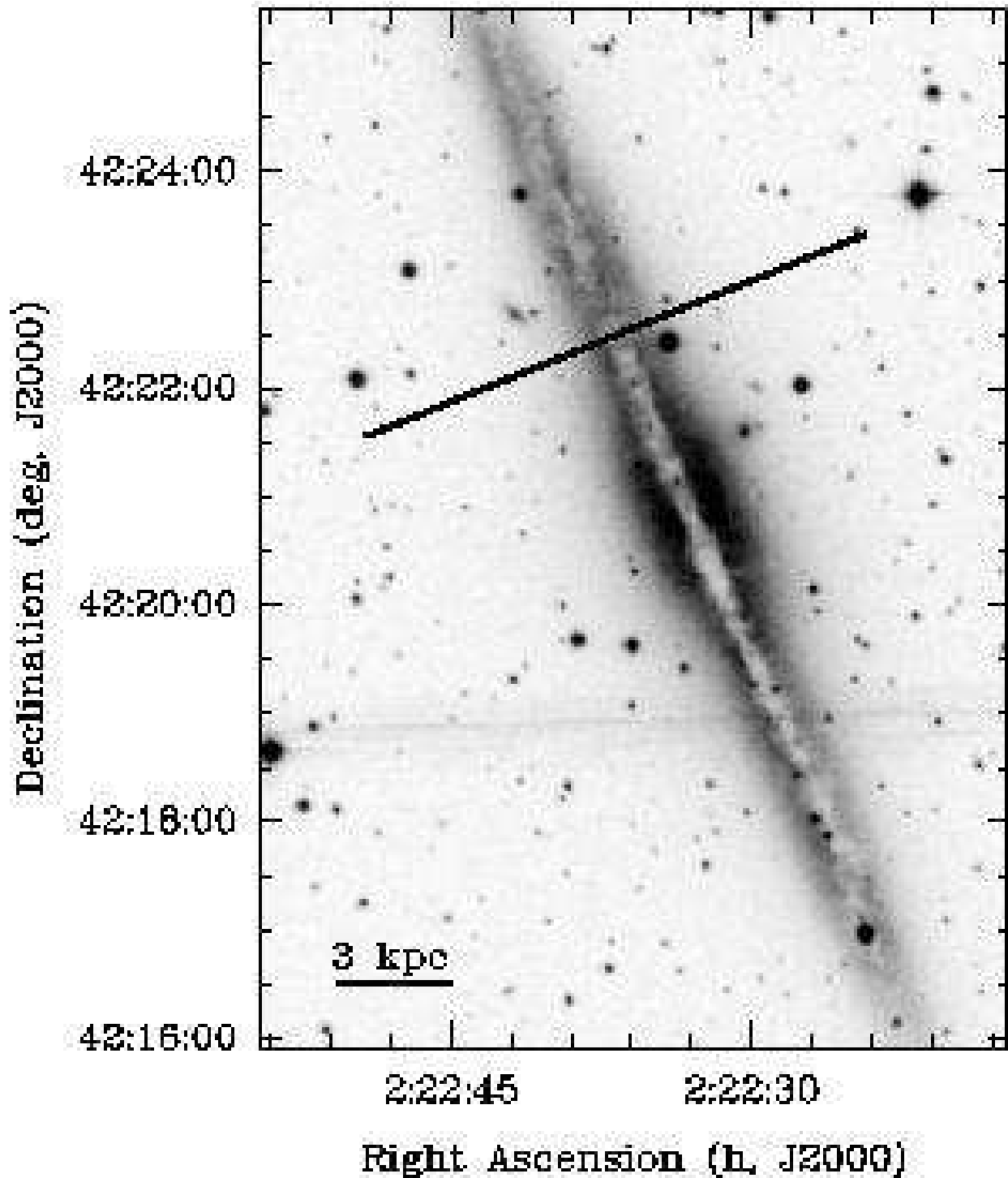


Fig. 1.— NGC 891 taken from the Digitized Sky Survey (Second Generation). The position of the slit is shown. In the following plots of NGC 891, positive numbers of parsecs refer to the right part of the slit counting westward, negative numbers refer to the left part of the slit counting eastward. We assumed a distance of 9.6 Mpc.

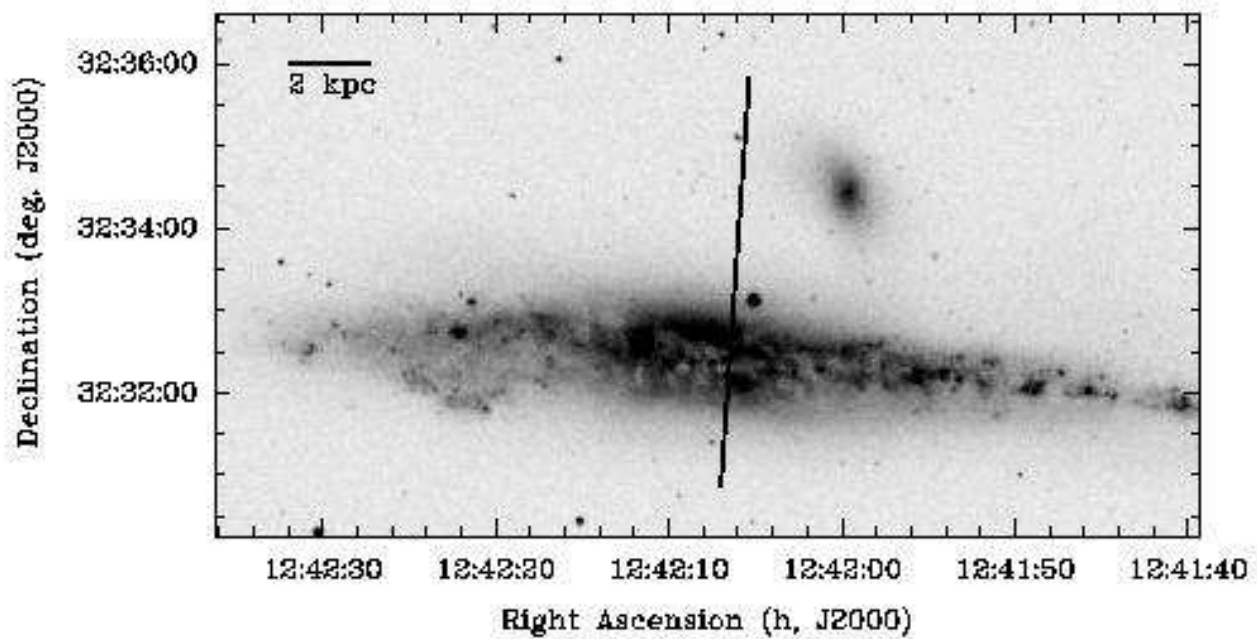


Fig. 2.— NGC 4631 taken from the Digitized Sky Survey (Second Generation). The position of the slit is shown. In the following plots of NGC 4631, positive numbers of parsecs refer to the upper part of the slit counting northward, negative numbers refer to the lower part of the slit counting southward. We assumed a distance of 6.9 Mpc.

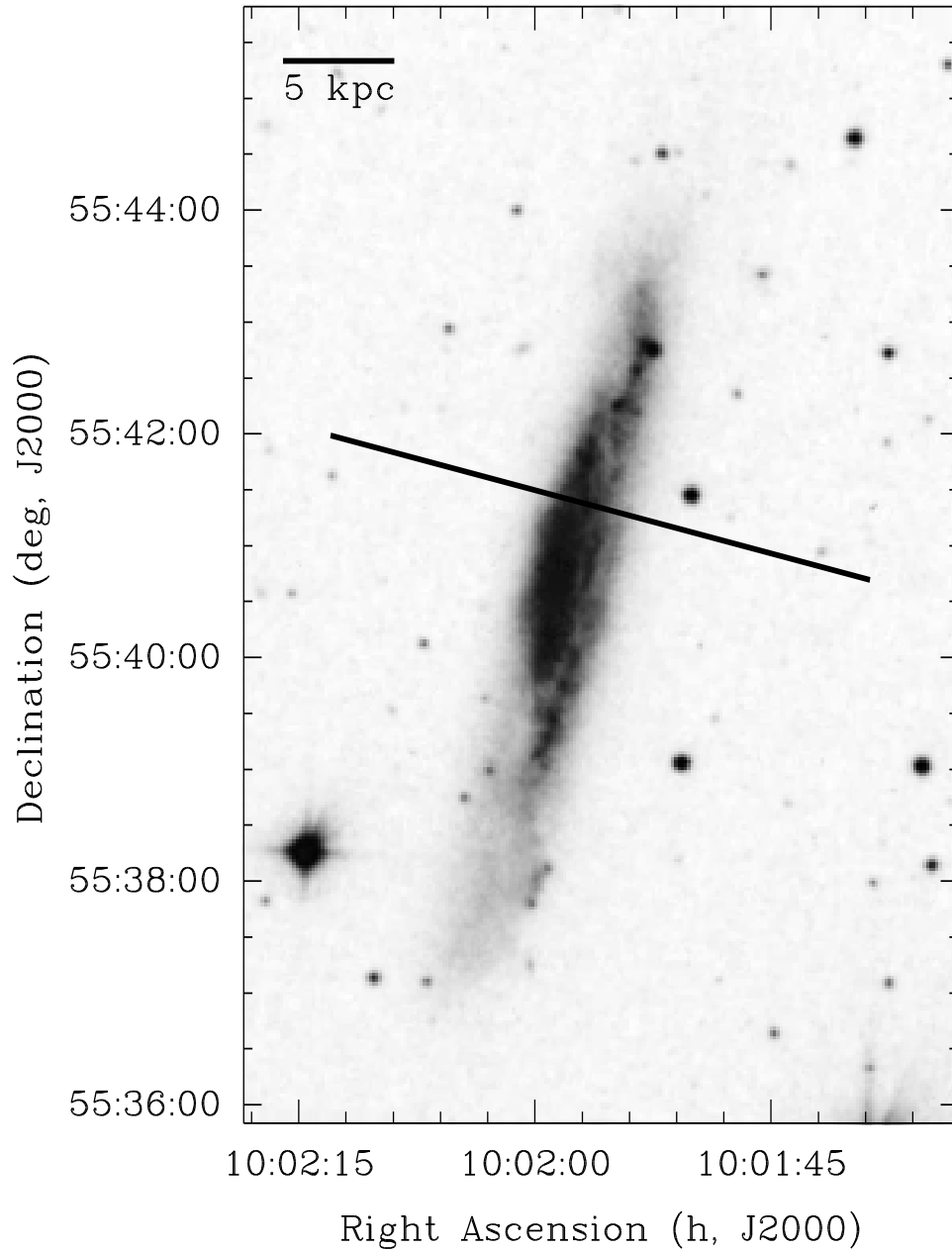


Fig. 3.— NGC 3079 taken from the Digitized Sky Survey (First Generation). The position of the slit is shown. In the following plots of NGC 3079, positive numbers of parsecs refer to the left part of the slit counting eastward, negative numbers refer to the right part of the slit counting westward. We assumed a distance of 17.3 Mpc.

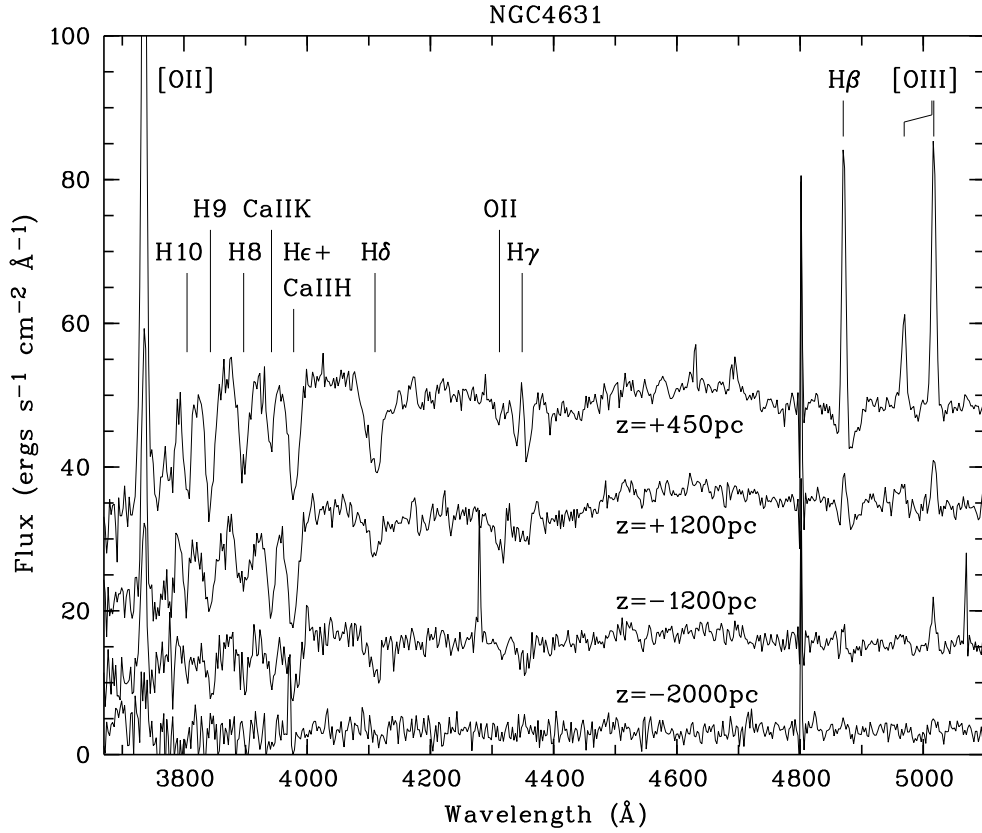


Fig. 4.— Blue part of the spectrum of NGC 4631. Four different rows of the longslit spectrum are shown. Each spectrum is an average of nine rows.  $H\gamma$  emission can clearly be seen at  $z = +450$  pc inside the  $H\gamma$  absorption line. The  $H\gamma$  emission disappears in the noise at  $|z| = 1200$  pc.  $H\beta$  emission can still be seen at  $z = -2000$  pc. The spectra also show that stellar continuum is clearly present at  $|z| = 1200$  pc.

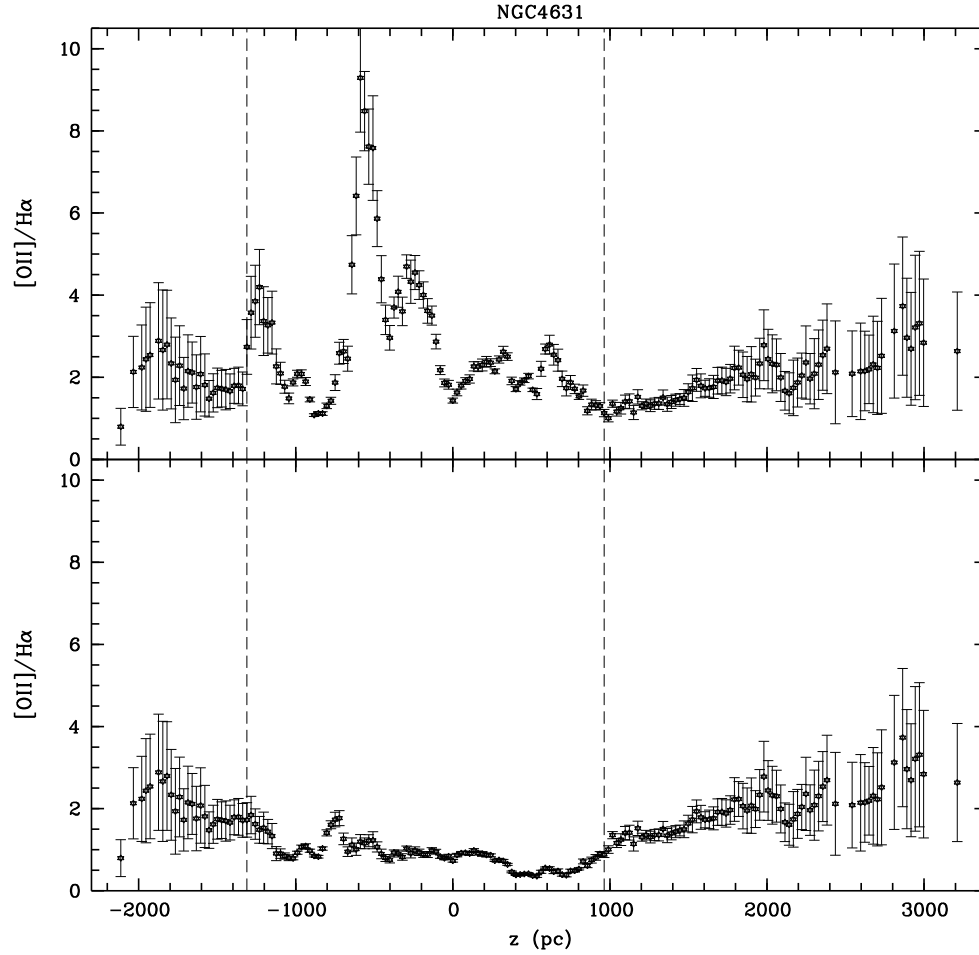


Fig. 5.—  $[\text{O II}]/\text{H}\alpha$  line ratio in NGC 4631. *Upper panel:*  $[\text{O II}]/\text{H}\alpha$  after extinction correction. *Lower panel:*  $[\text{O II}]/\text{H}\alpha$  without extinction correction. The *dashed lines* show the range affected by the extinction correction. It is not clear how physical the peaks in the midplane are.

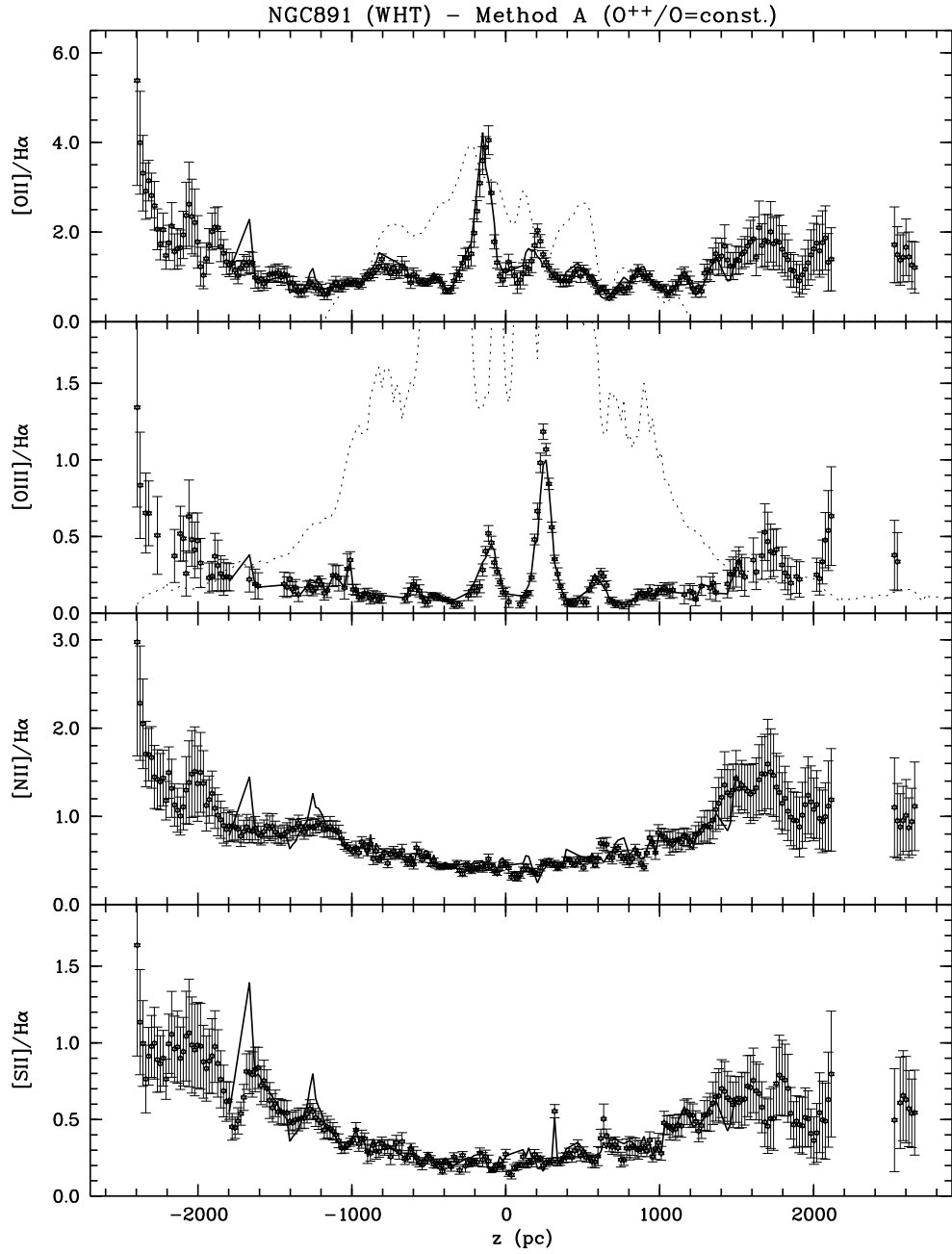


Fig. 6.—  $H\alpha$  line ratios and derived properties of NGC 891 using Method A ( $O^{++}/O = \text{const.}$ ). (a) The measured  $H\alpha$  line ratios are compared with the predicted line ratios (*solid lines*). Only the predictions for  $O^{++}/O = 0.15$  are shown. The *dotted line* in the *top panel* shows the derived optical depth  $\tau$  (unscaled). The *dotted line* in the *second from top panel* shows the  $H\alpha$  intensity along the slit scaled down to fit the plot. (b) The derived electron temperature, oxygen and nitrogen abundance, and sulfur ionization fraction are shown for the four different oxygen ionization fractions  $O^{++}/O = 0.05, 0.10, 0.15, 0.20$ . The arrows with the attached numbers indicate the maximum values reached, but not shown in the plot.

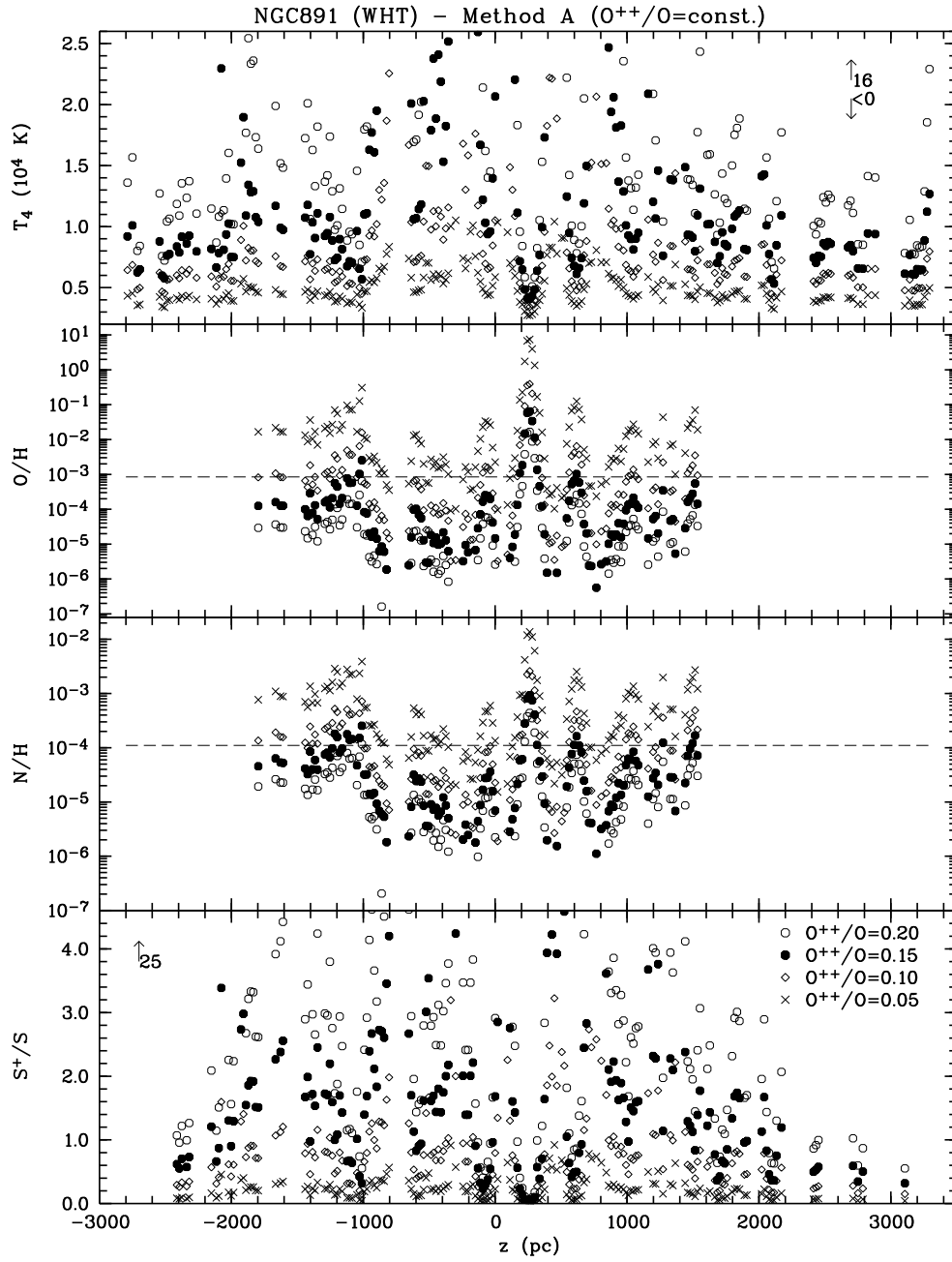


Fig. 6b.—

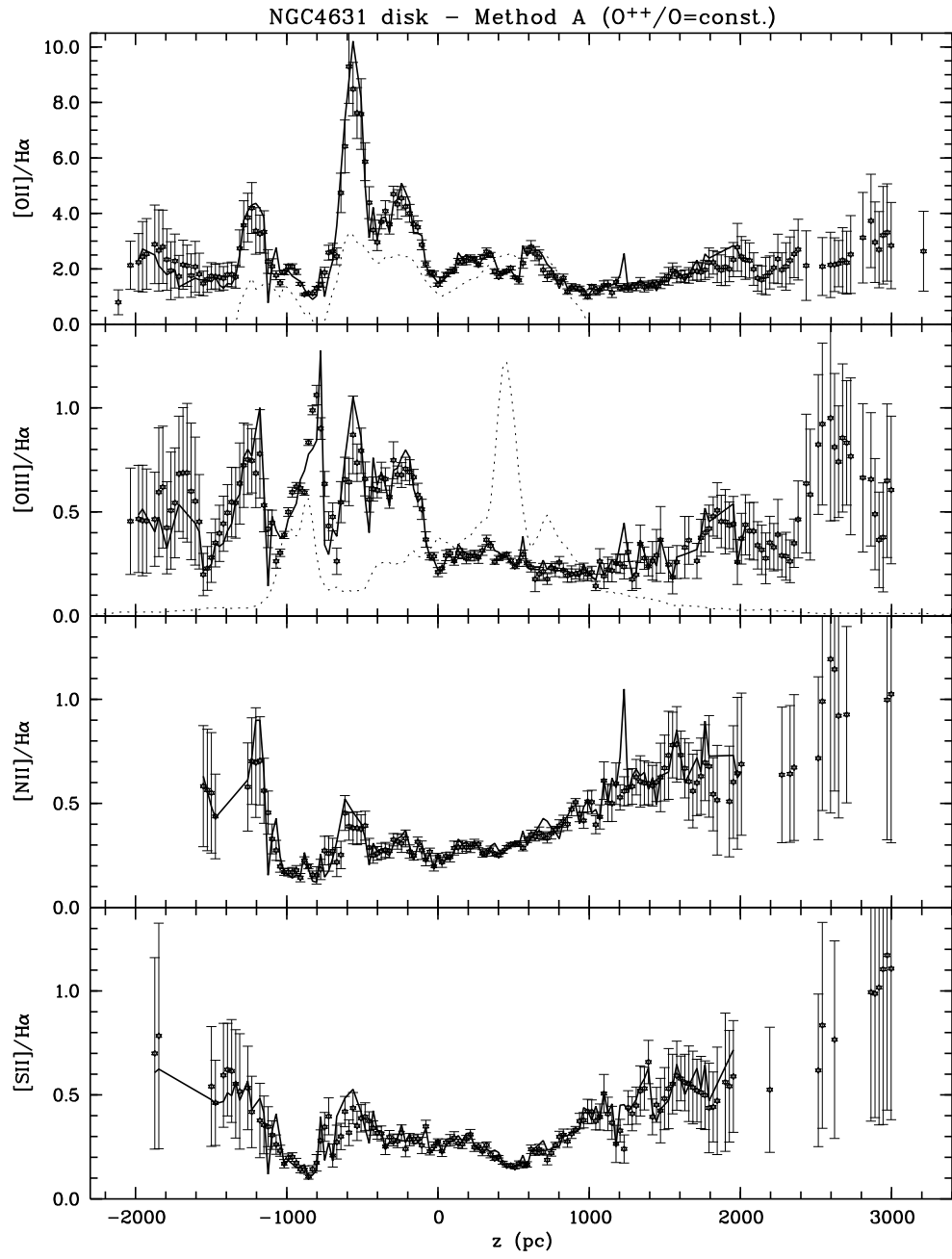


Fig. 7.— Same as Fig. 6, but for NGC 4631.

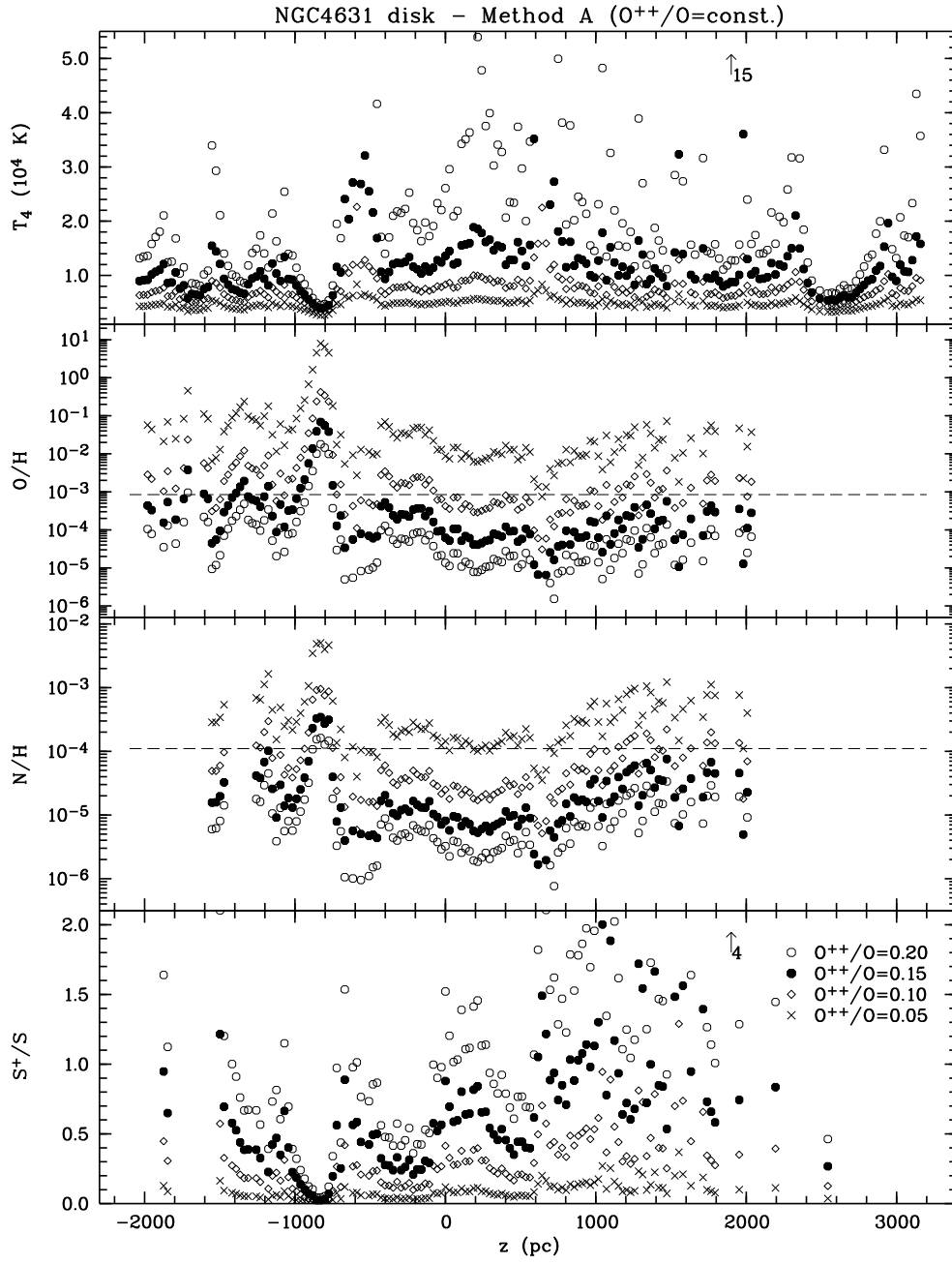


Fig. 7b.—

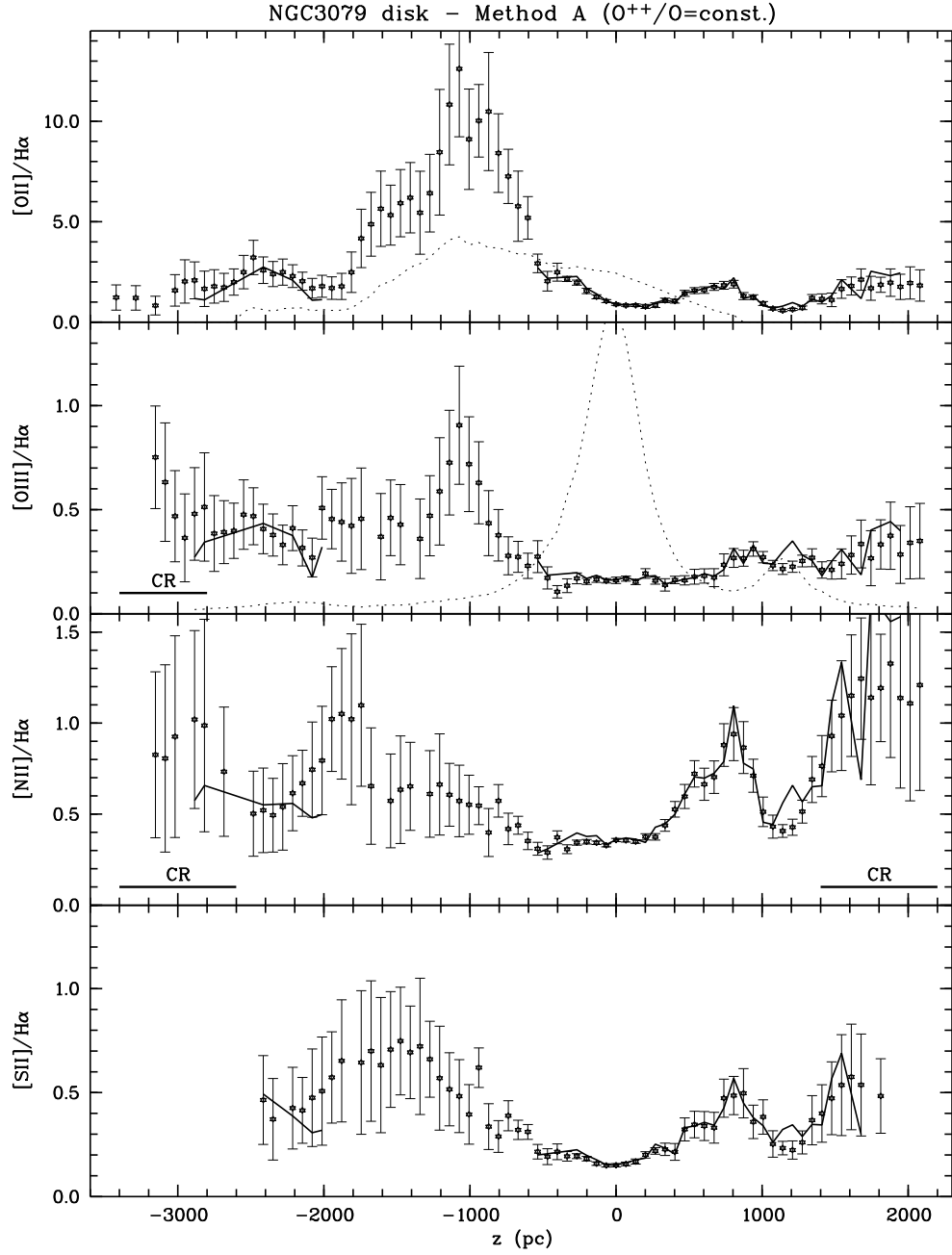


Fig. 8.— Same as Fig. 6, but for NGC 3079. Data contaminated by cosmic ray hits are marked with the bars labeled “CR”.

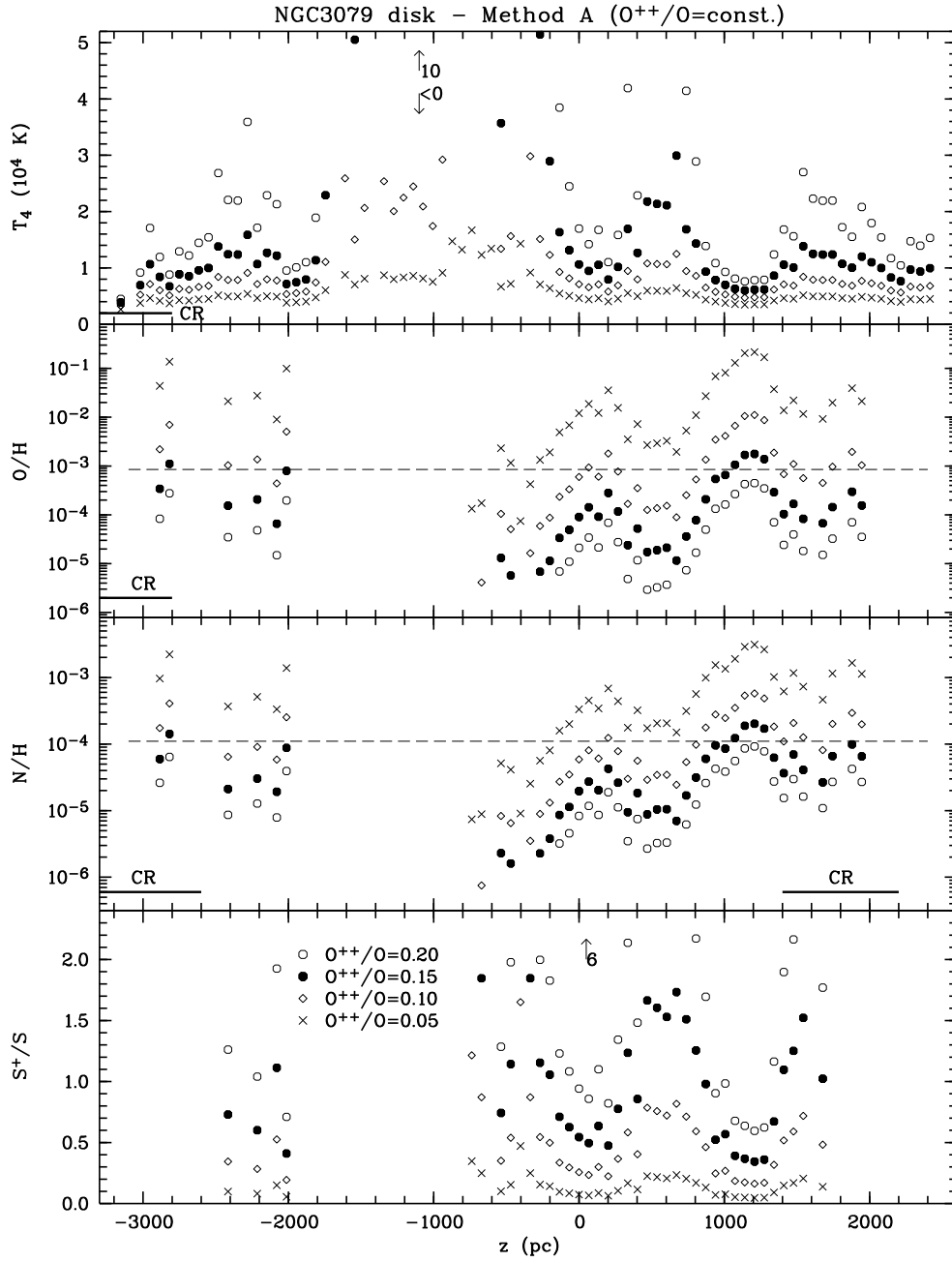


Fig. 8b.—

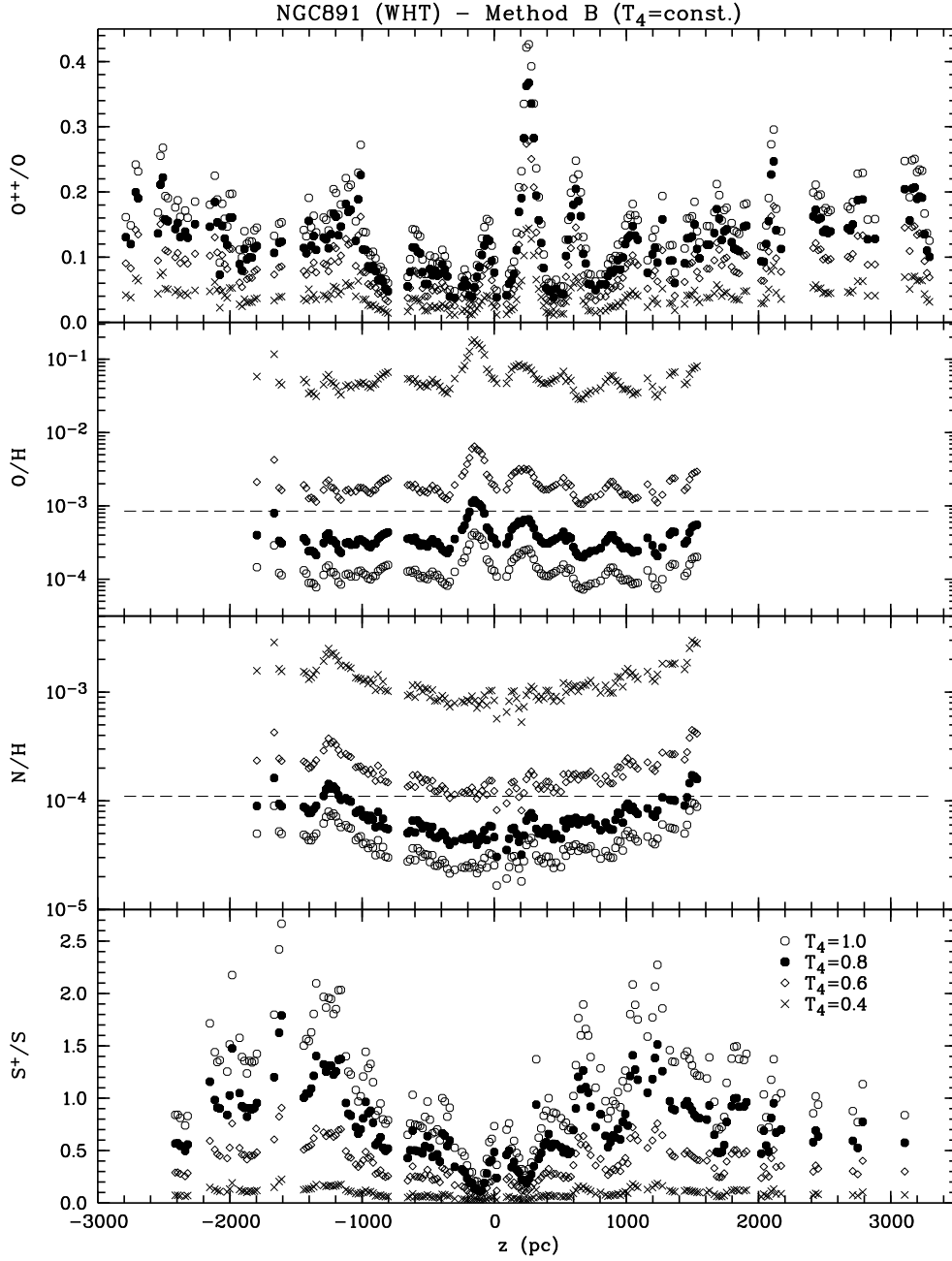


Fig. 9.— Derived properties of NGC 891 using Method B ( $T_4 = \text{const.}$ ). The derived ionization fraction of doubly ionized oxygen, the oxygen and nitrogen abundance, and the sulfur ionization fraction are shown for the four different temperatures  $T_4 = 0.4, 0.6, 0.8, 1.0$  ( $T_4$  measured in 10 000 K).

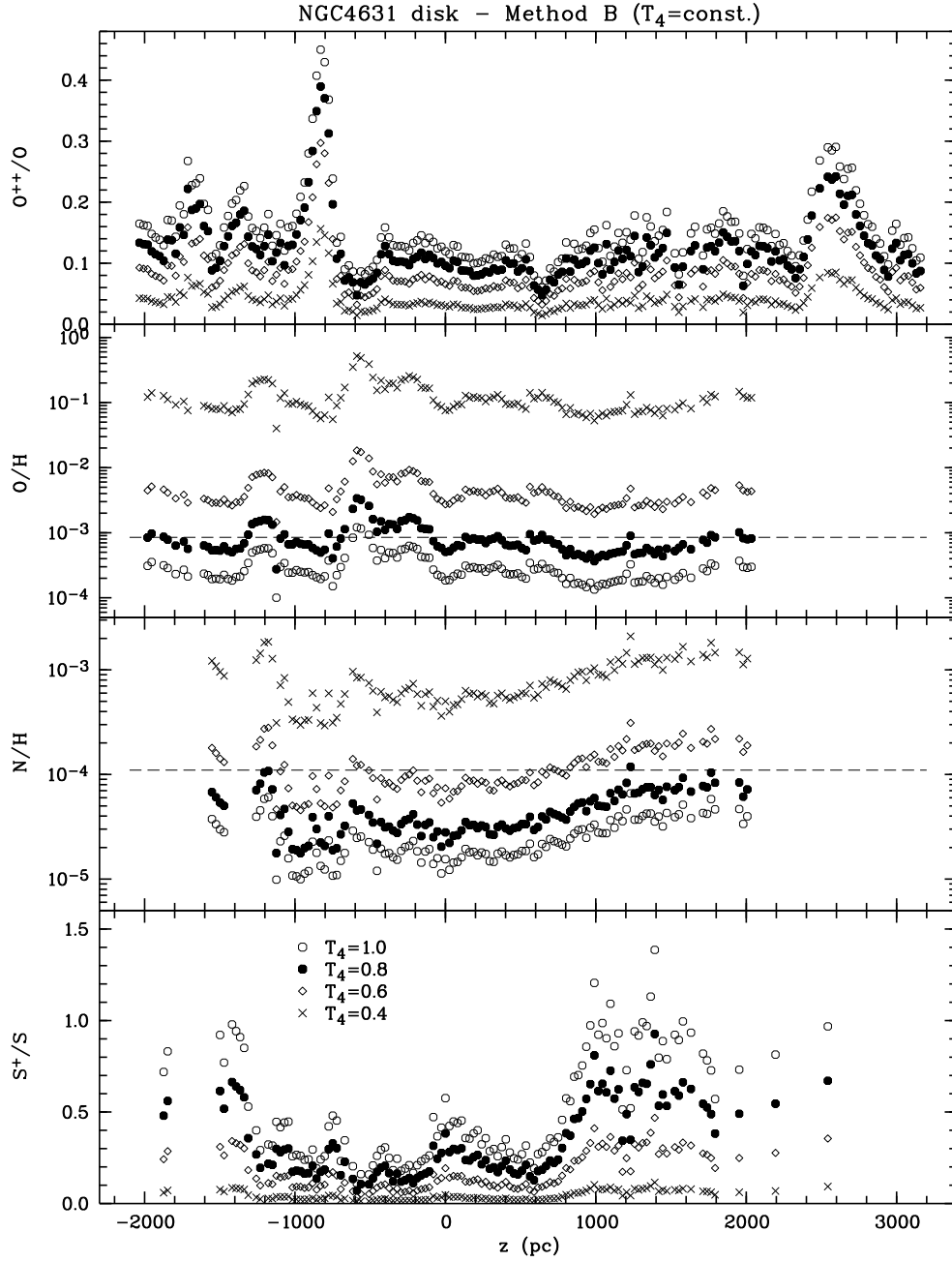


Fig. 10.— Same as Fig. 9, but for NGC 4631.

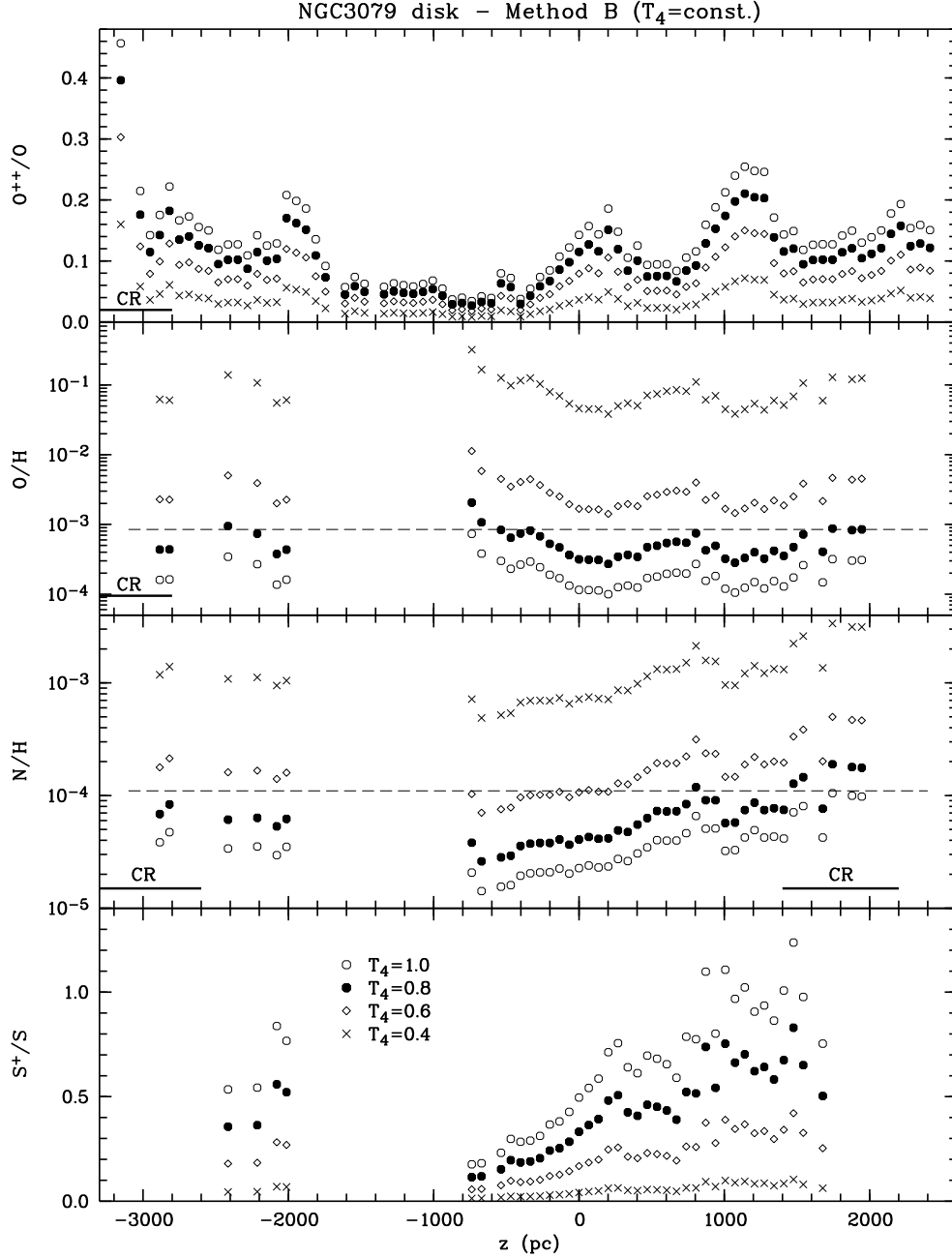


Fig. 11.— Same as Fig. 9, but for NGC 3079. Data contaminated by cosmic ray hits are marked with the bars labeled “CR”.

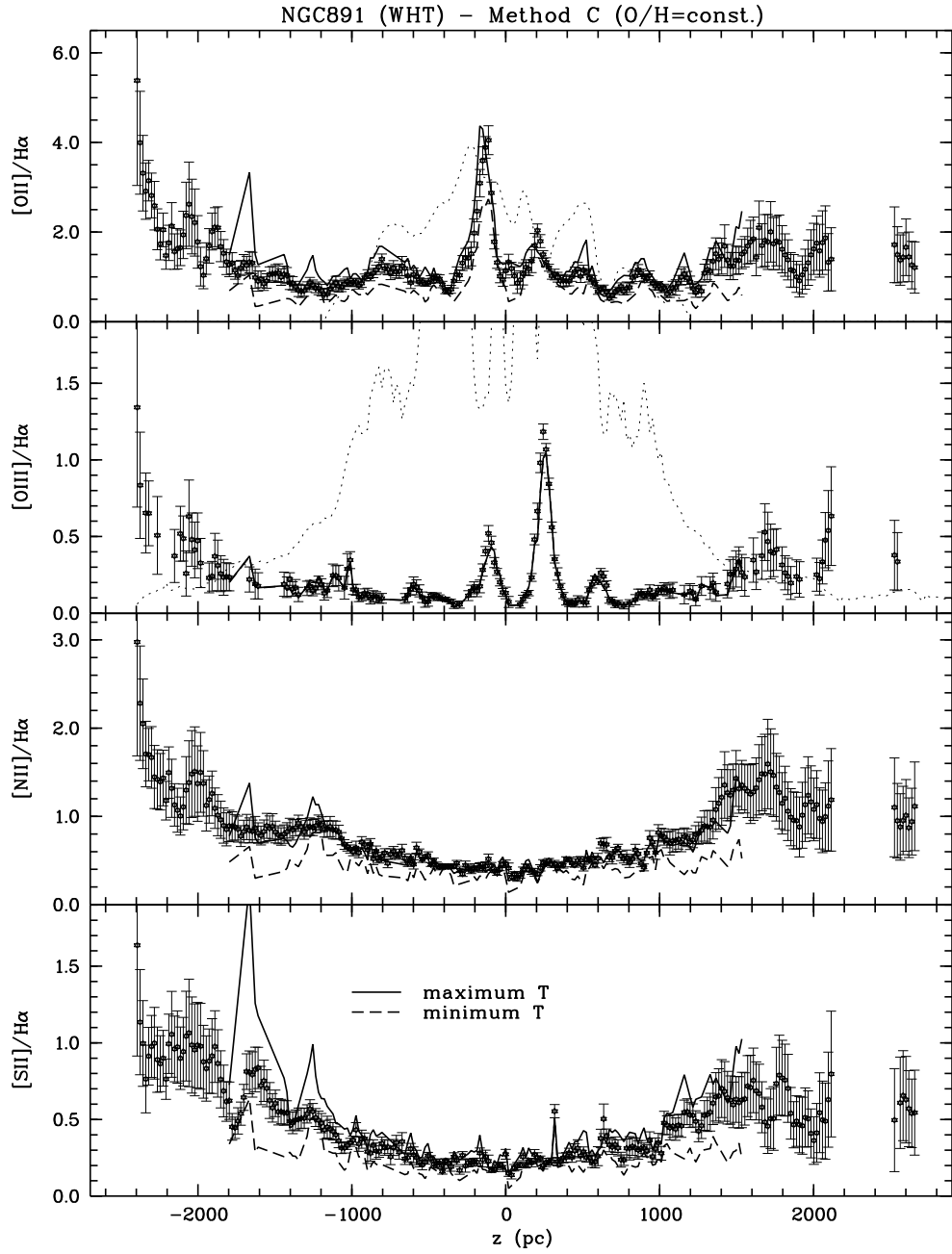


Fig. 12.—  $H\alpha$  line ratios and derived properties of NGC 891 using Method C ( $O/H = \text{const.}$ ). (a) The measured  $H\alpha$  line ratios are compared with the predicted line ratios using the maximum temperature (*solid lines*) and the minimum temperature (*dashed lines*). The *dotted line* in the *top panel* shows the derived optical depth  $\tau$  (unscaled). The *dotted line* in the *second from top panel* shows the  $H\alpha$  intensity along the slit scaled down to fit the plot. (b) The derived electron temperature, ionization fraction of doubly ionized oxygen, the nitrogen abundance, and the sulfur ionization fraction are shown for both the maximum temperature (*filled circles*) and the minimum temperature (*open diamonds*). (c) same as (a), but without extinction correction. (d) same as (b), but without extinction correction.

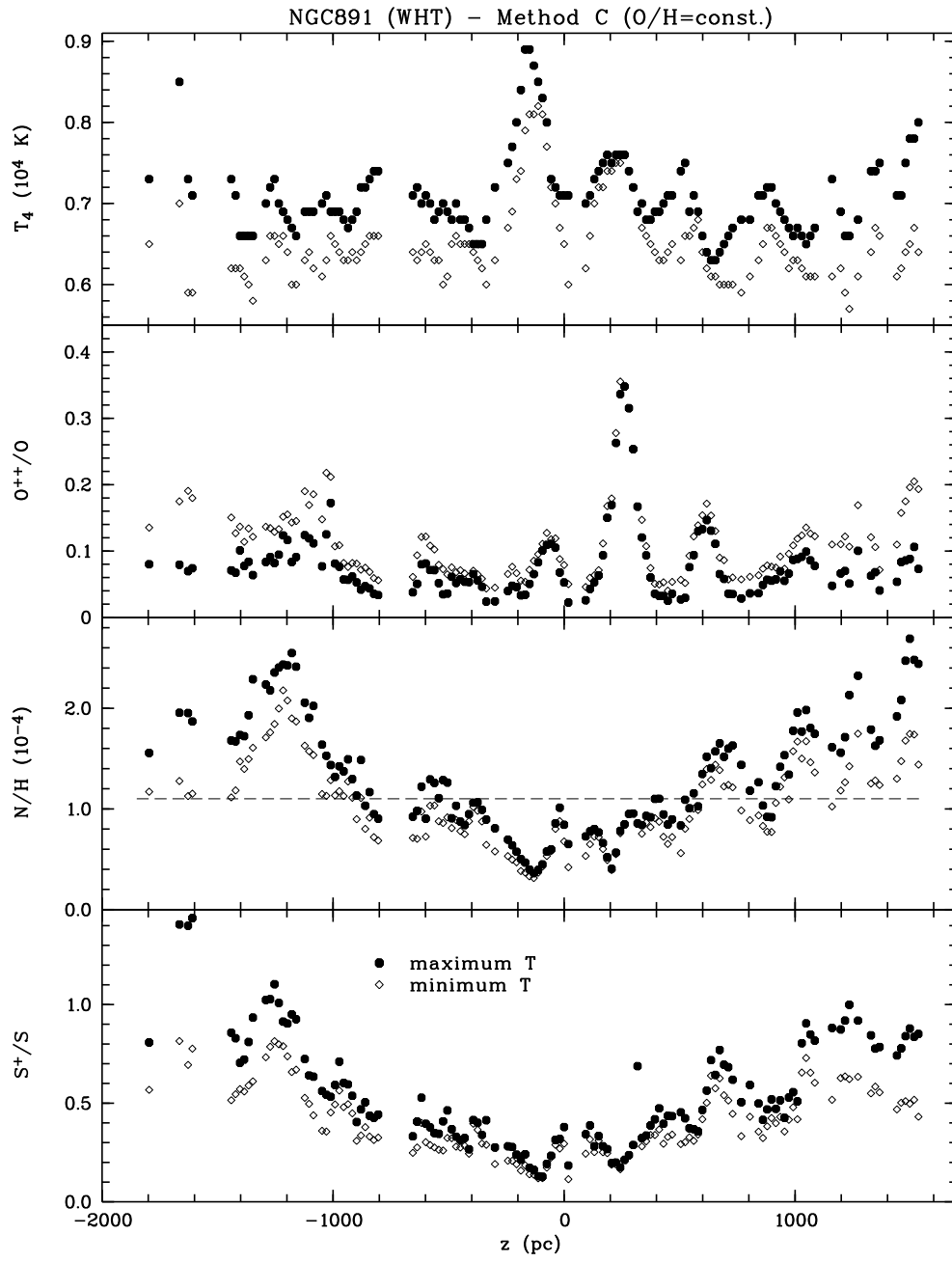


Fig. 12b.—

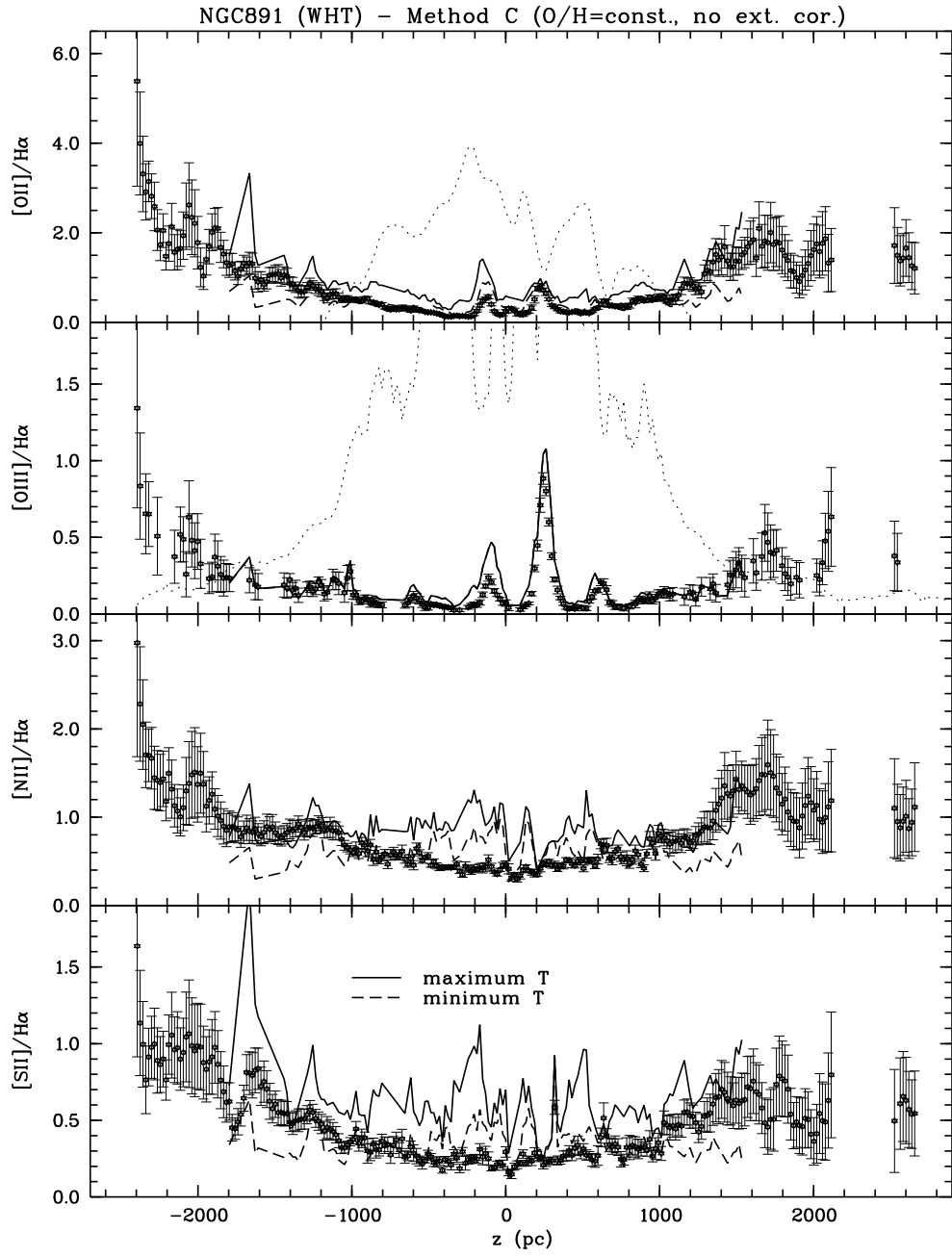


Fig. 12c.—

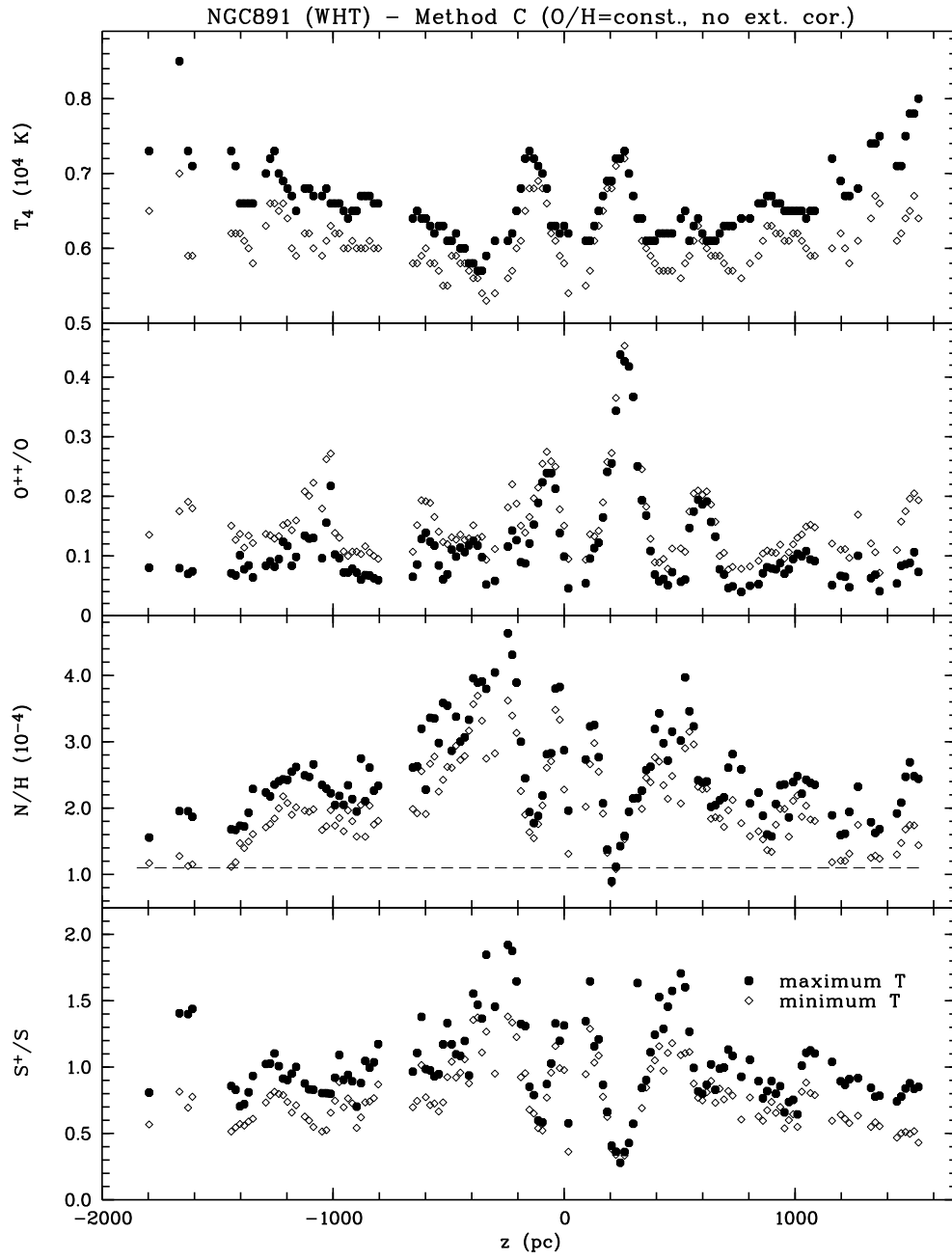


Fig. 12d.—

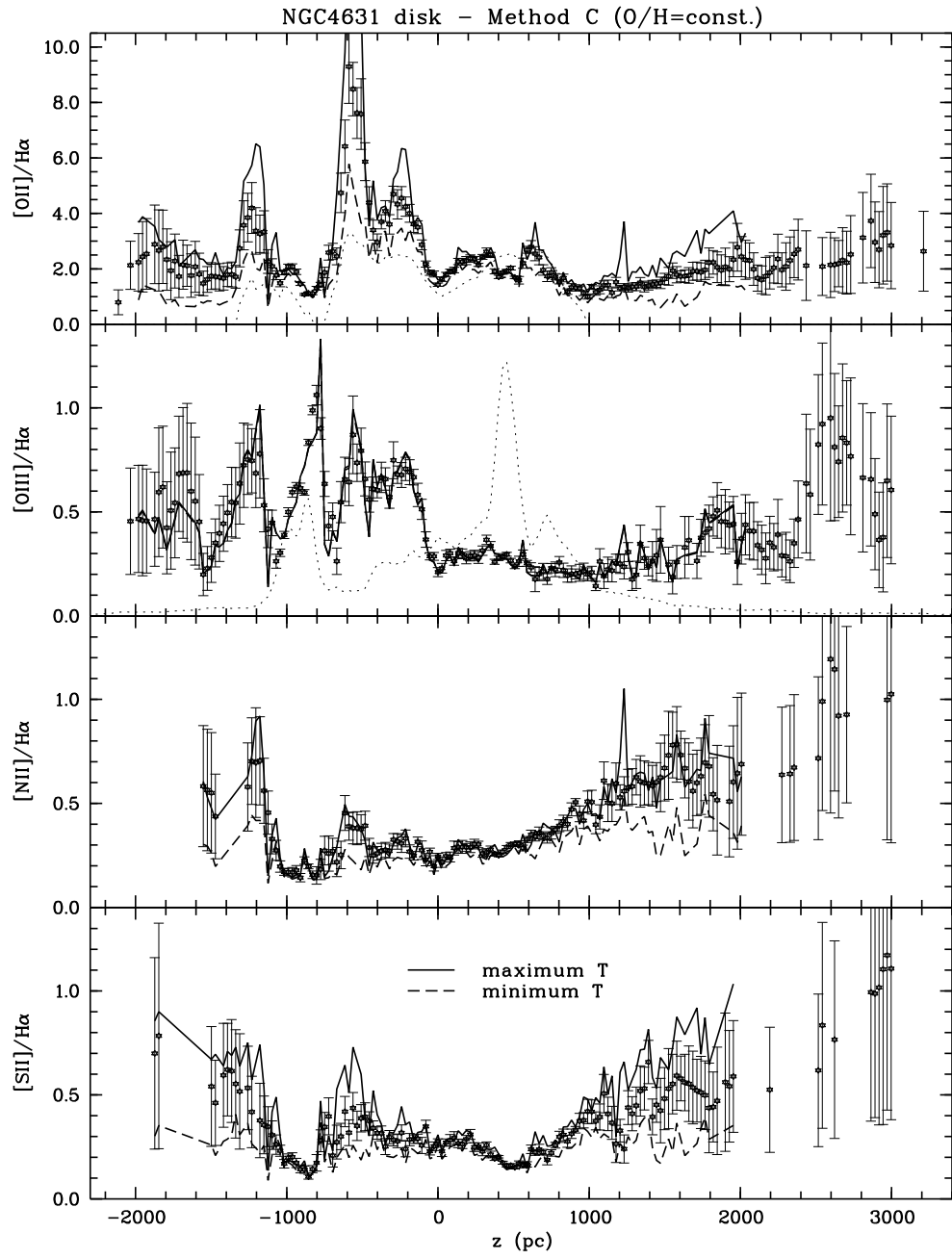


Fig. 13.— Same as Fig. 12, but for NGC 4631.

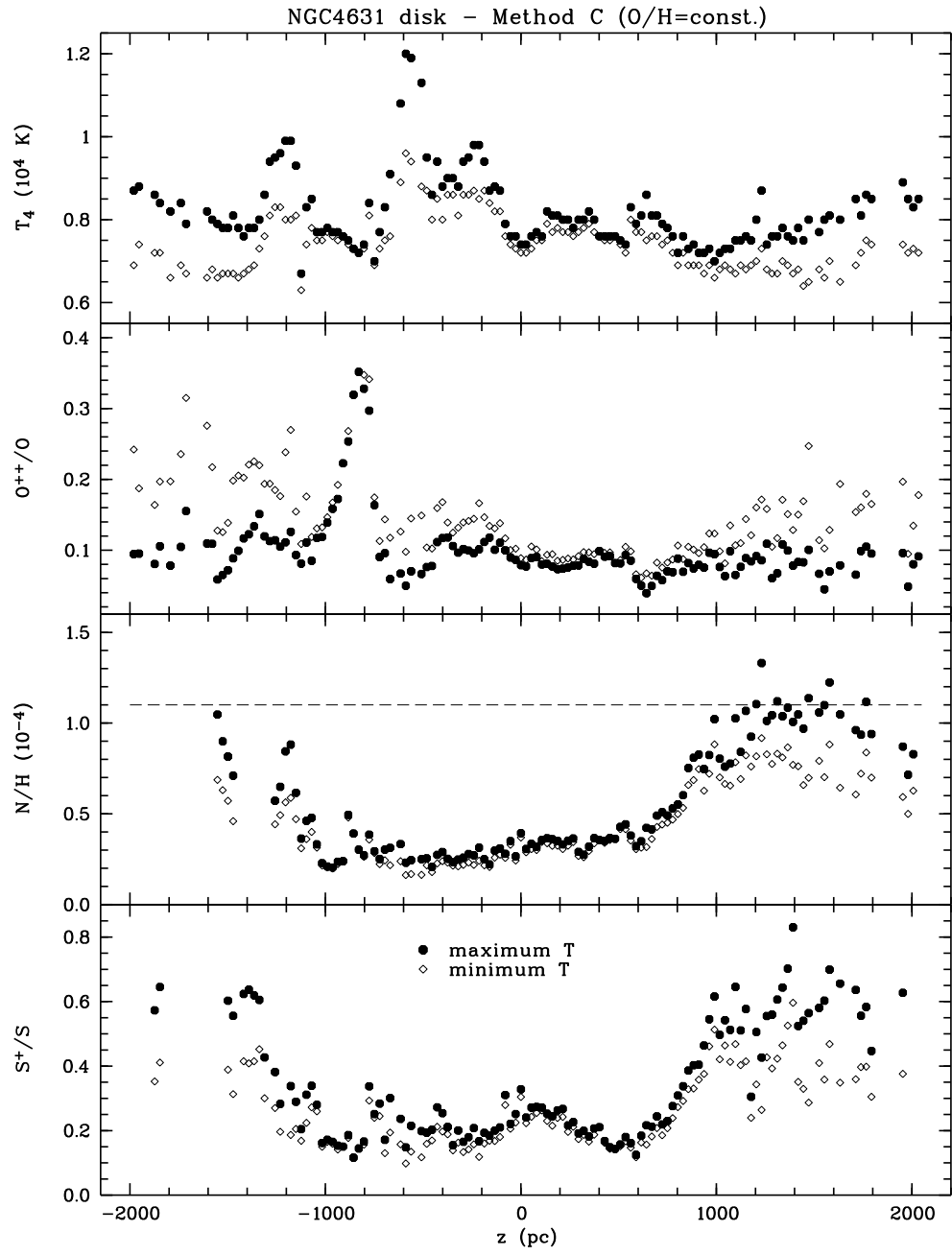


Fig. 13b.—

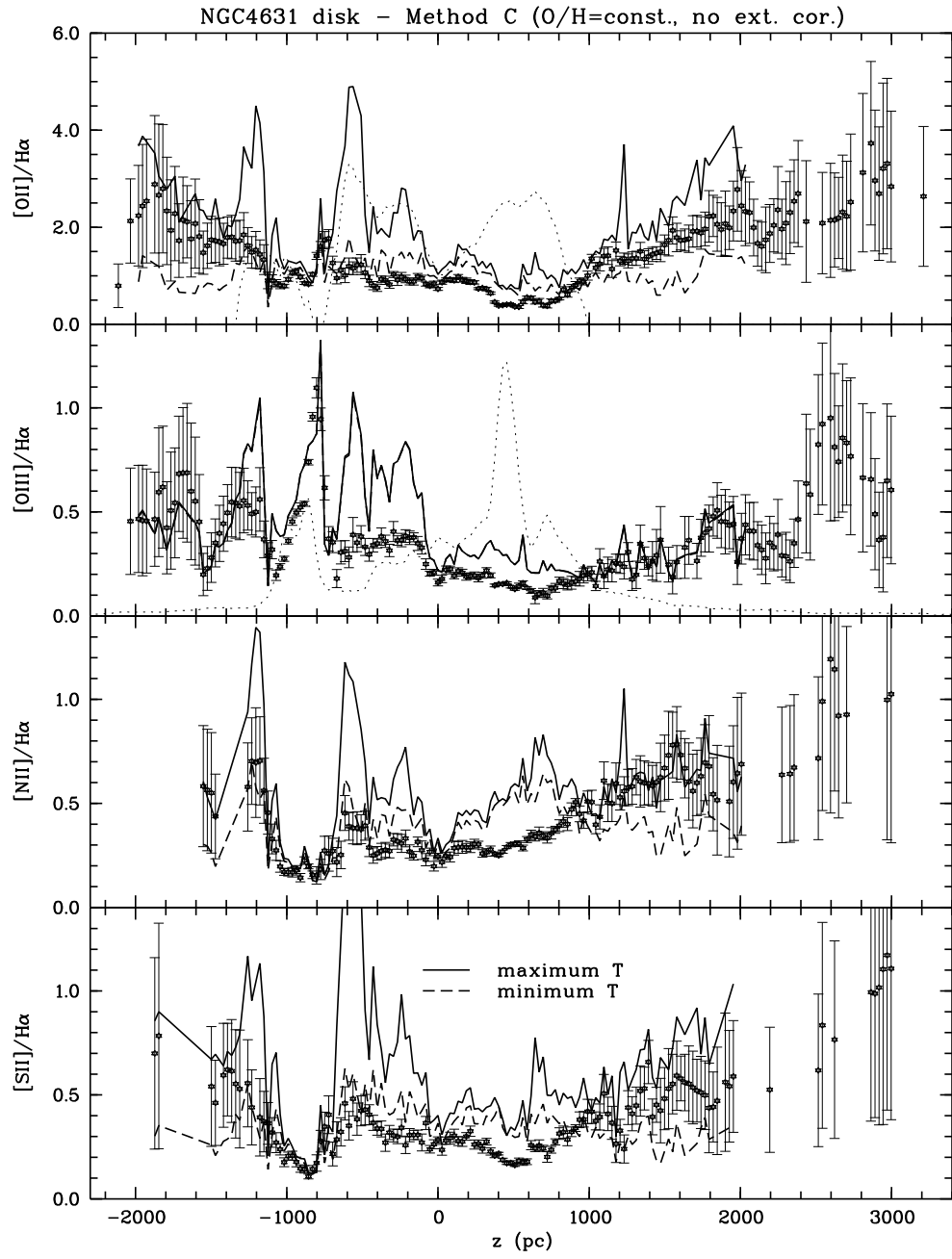


Fig. 13c.—

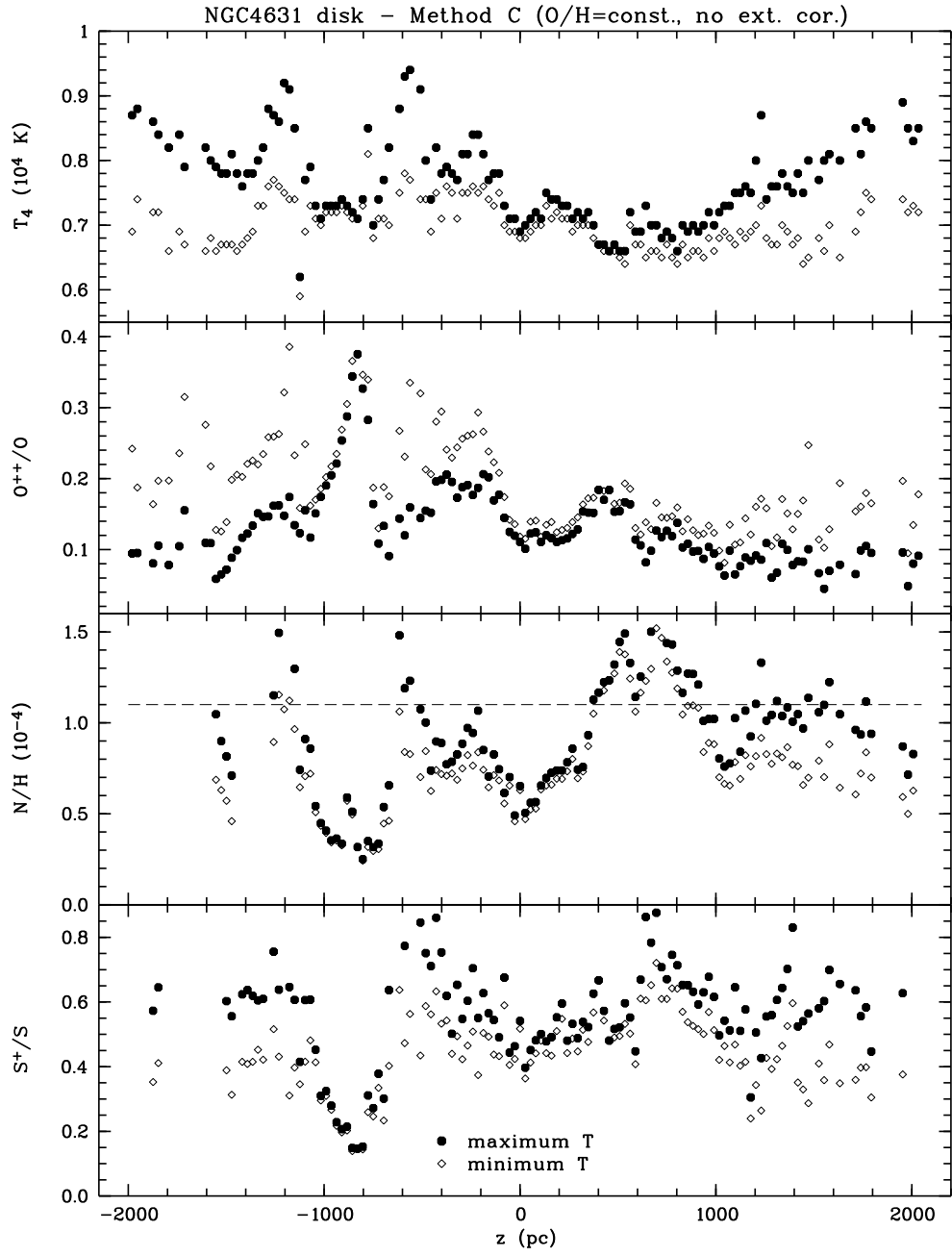


Fig. 13d.—

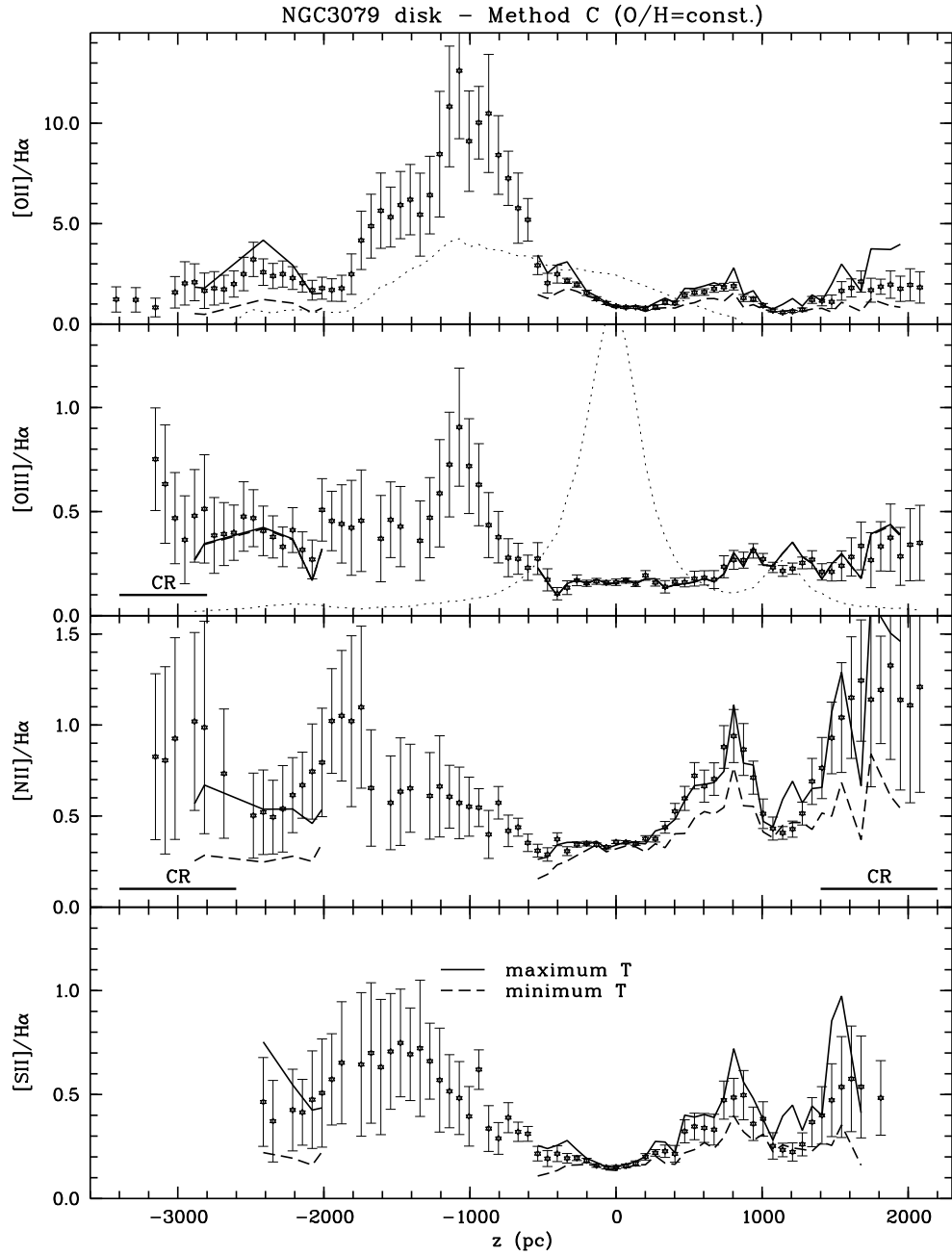


Fig. 14.— Same as Fig. 12, but for NGC 3079. Data contaminated by cosmic ray hits are marked with the bars labeled “CR”.

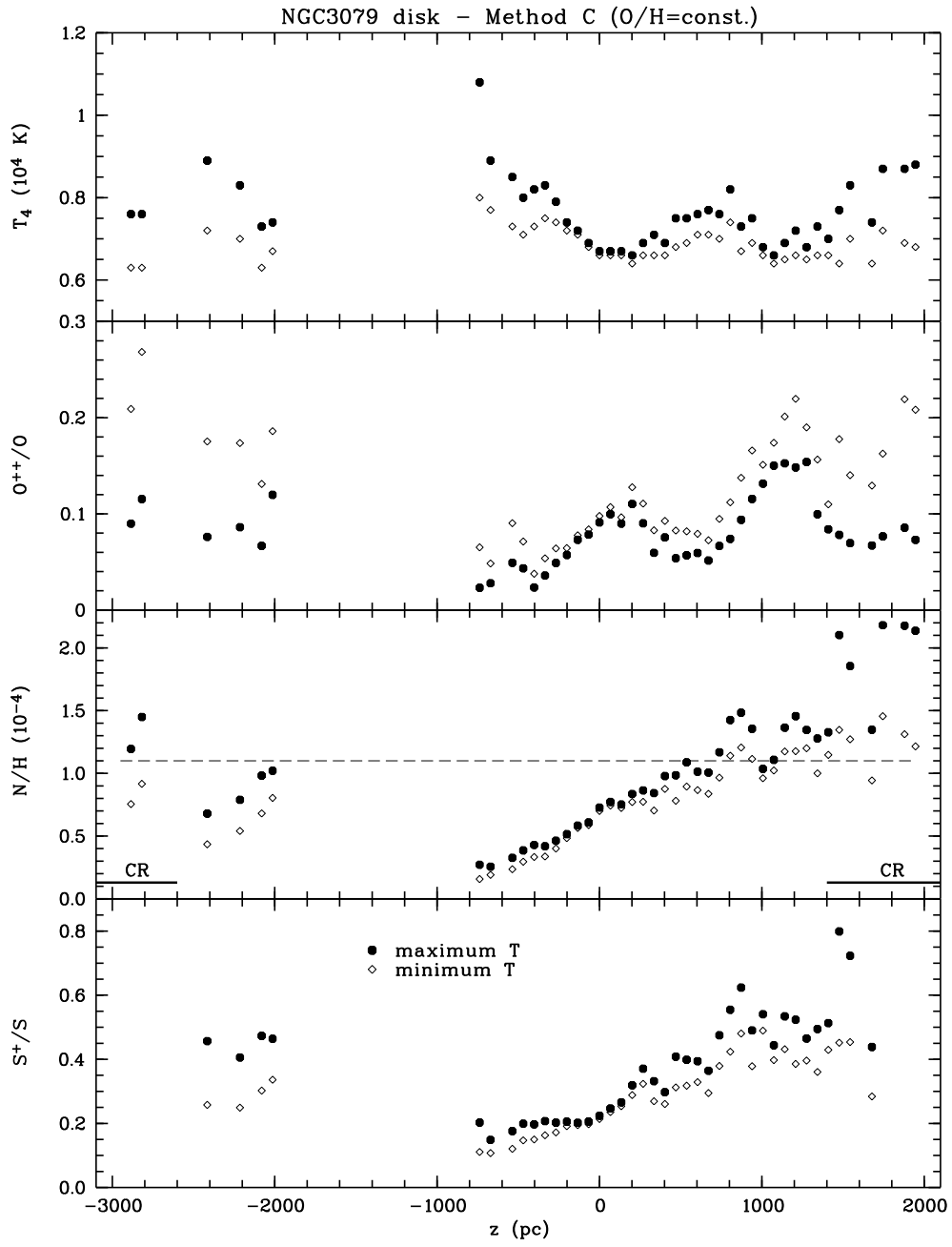


Fig. 14b.—

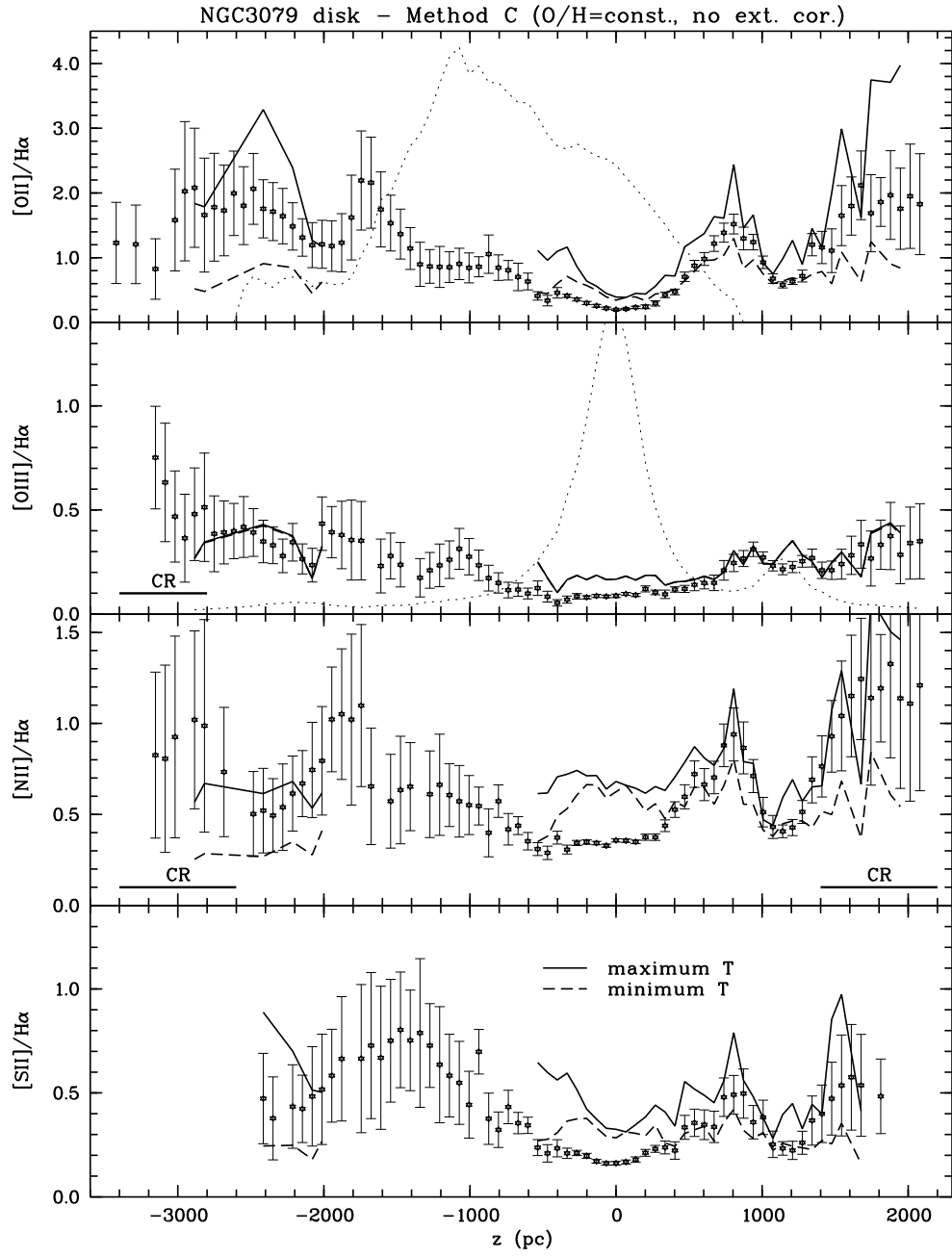


Fig. 14c.—

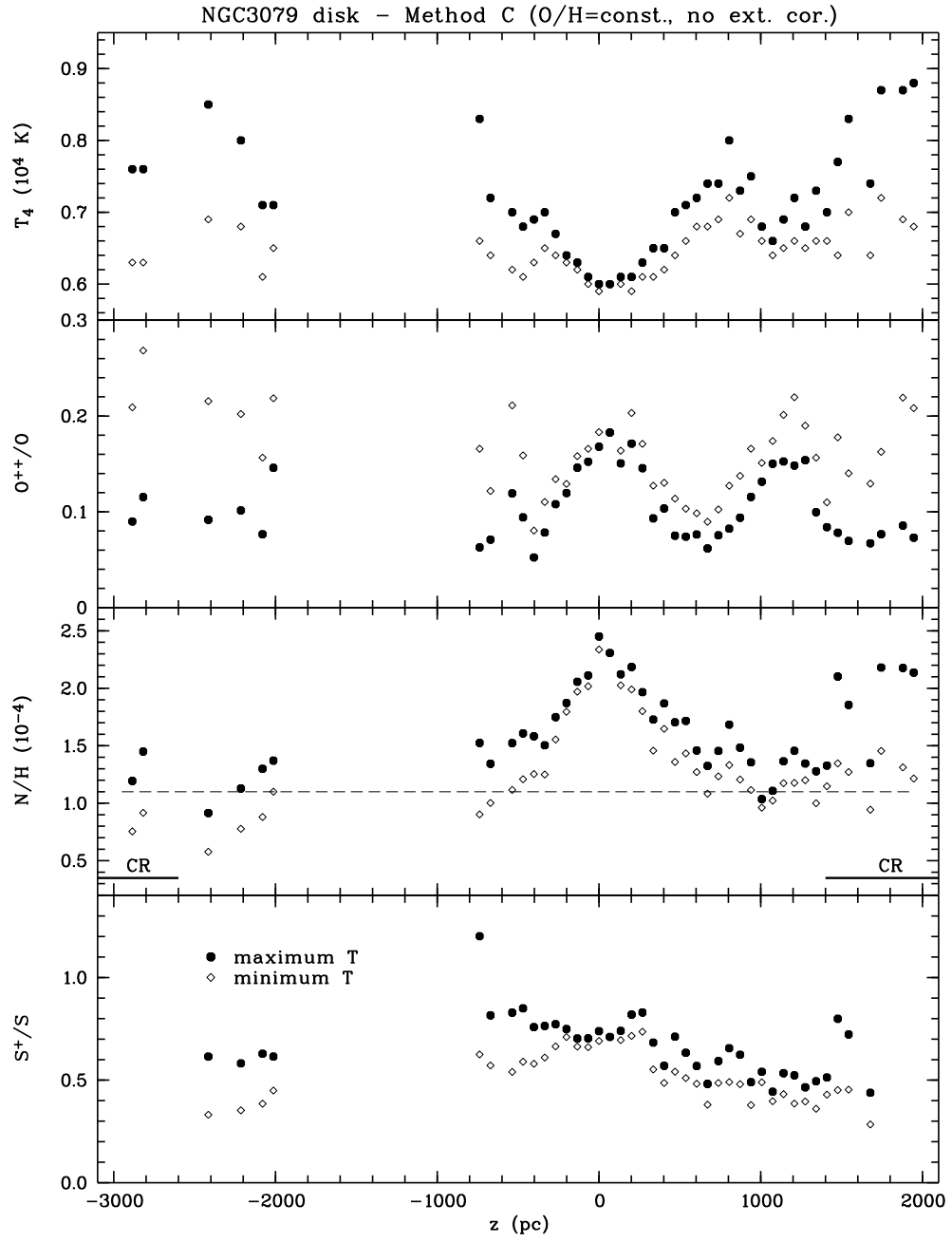


Fig. 14d.—

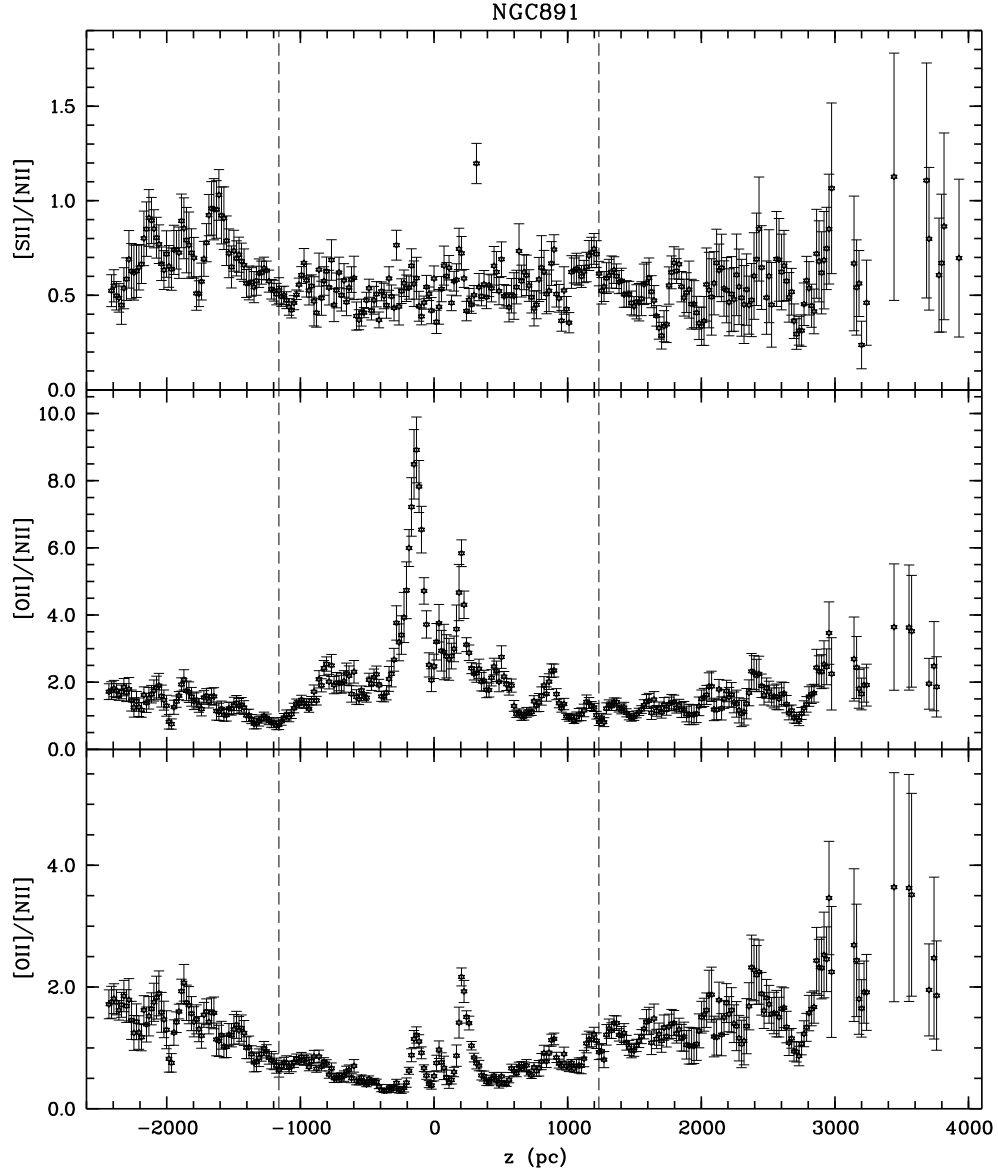


Fig. 15.—  $[S\ II]/[N\ II]$  and  $[O\ II]/[N\ II]$  line ratios for NGC 891. *Top panel:*  $[S\ II]/[N\ II]$  (extinction corrected). *Middle panel:*  $[O\ II]/[N\ II]$  (extinction corrected). *Bottom panel:*  $[O\ II]/[N\ II]$  (without extinction correction). The *dashed lines* show the range affected by the extinction correction.

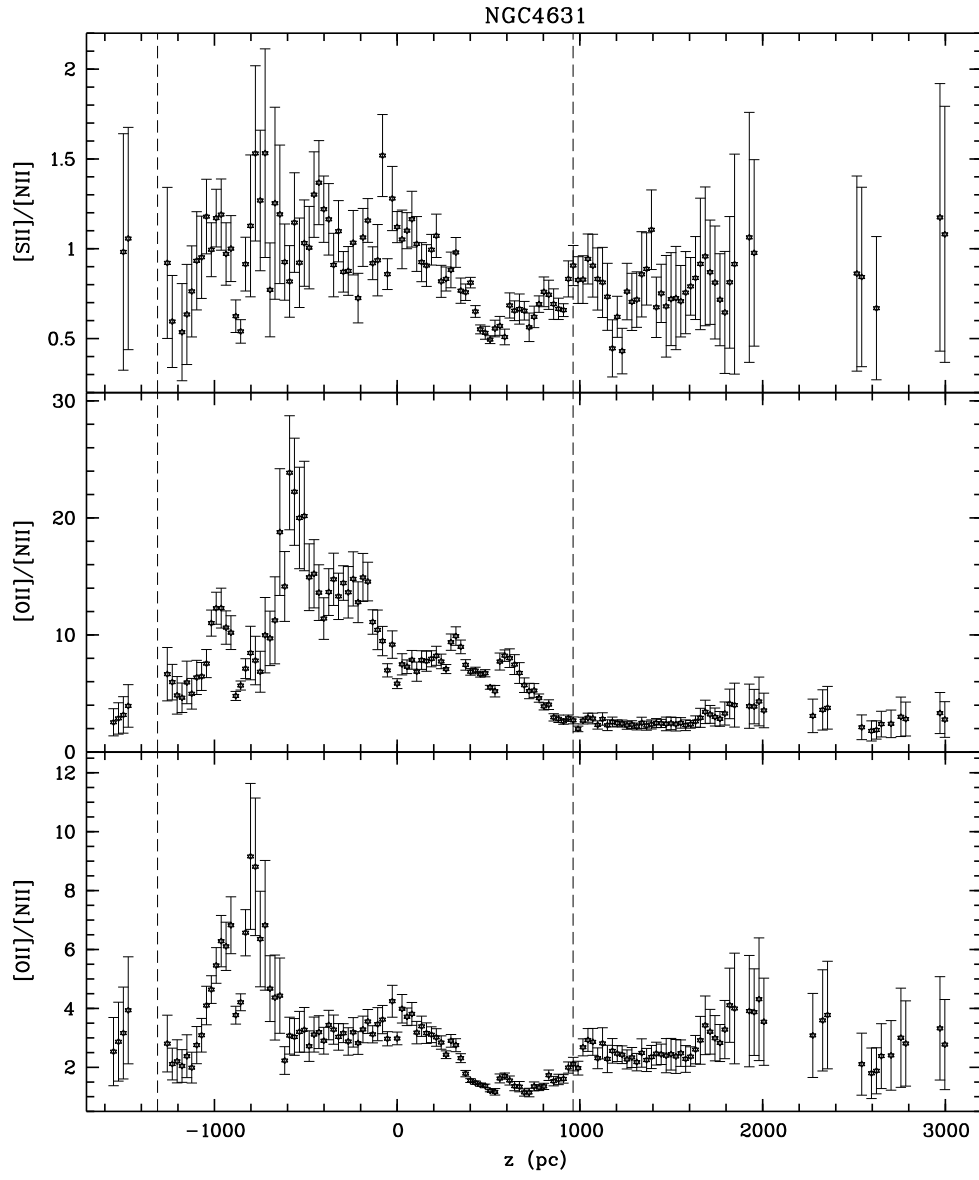


Fig. 16.— Same as Fig. 15, but for NGC 4631.

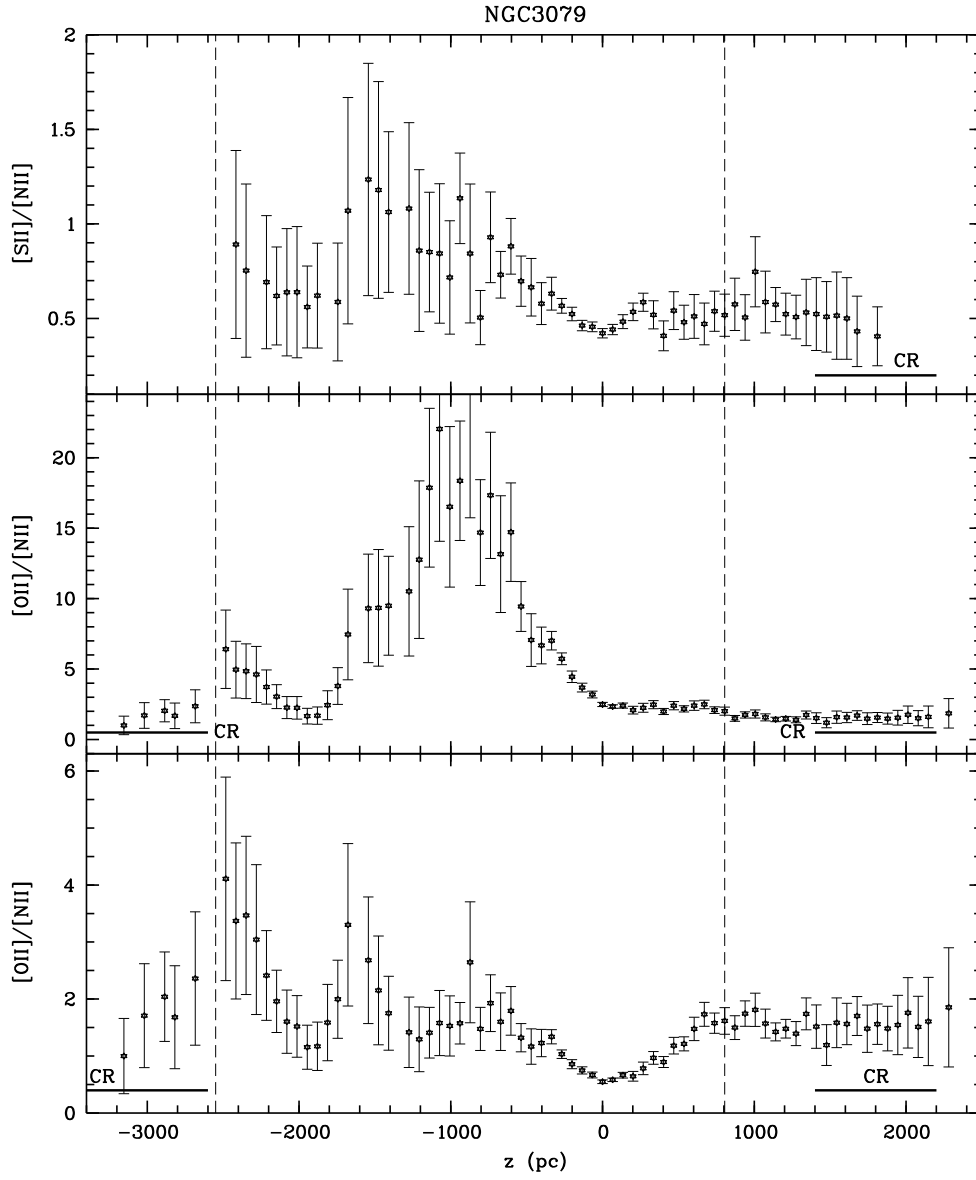


Fig. 17.— Same as Fig. 15, but for NGC 3079. Data contaminated by cosmic ray hits are marked with the bars labeled “CR”.